UNIVERSITY OF THE AEGEAN

INFORMATION AND COMMUNICATION SYSTEMS ENGINEERING DEPARTMENT

Numerical study of a Two-Section Quantum-Well Laser and neuron based autaptic memory system.

Thesis diploma

of

Tzeka Nikolaos

Supervisor : Charis Mesaritakis

Committee members: Kostoulas Theodoros, Kalligeros Emmanouil

Samos, 15st March 2024

Acknowledgements

I want to thank my spinal cord for supporting me for so many years.

Tzeka Nikolaos

Information and Communications system Engineering

UNIVERSITY OF THE AEGEAN

Table of Contents

Abbreviations

DE	Differential Equation
SDE	Second Order Differential Equation
AI	Artificial Intelligence
NN	Neural Network
SNN	Spiking Neural Network
SOA	Semiconductor Optical Amplification
LIF	Leaky-Integrade-Fire

Summary

In the era of big data, the volume of data continues to escalate, presenting challenges and opportunities for artificial intelligence (AI) applications. Advancements in AI technologies are accelerating at an unprecedented rate, with continuous improvements in machine learning algorithms. Inspired by the remarkable efficiency of the human brain, researchers have turned to spiking neural network (SNN) algorithms as a more efficient alternative for machine learning tasks. Unlike traditional approaches, SNNs offer enhanced efficiency and effectiveness in processing complex data sets.

The limitations of old silicon chips in accommodating modern machine learning algorithms have prompted the exploration of alternative hardware solutions. Laser technology has emerged as a promising candidate, given its inherent spiking behavior analogous to biological neurons. Additionally, lasers offer superior speed and efficiency, bypassing issues such as leakage current[14] and the need to charge parasitic capacities, thereby eliminating the fanout problem. This convergence of neuroscience-inspired algorithms and laser technology presents a compelling avenue for advancing the capabilities of AI systems.

Greek

Στην εποχή των μεγάλων δεδομένων, ο όγκος των δεδομένων συνεχίζει να αυξάνεται, παρουσιάζοντας προκλήσεις και ευκαιρίες για εφαρμογές τεχνητής νοημοσύνης (ΤΝ). Οι πρόοδοι στις τεχνολογίες ΤΝ επιταχύνονται με ασυνήθιστο ρυθμό, με συνεχείς βελτιώσεις στους αλγόριθμους μηχανικής μάθησης. Εμπνευσμένοι από την εξαιρετική απόδοση του ανθρώπινου εγκεφάλου, οι ερευνητές έχουν στραφεί στους αλγόριθμους των εκρήξεων νευρώνων (SNN) ως μια πιο αποδοτική εναλλακτική για τις εργασίες μάθησης των μηχανών. Σε αντίθεση με τις παραδοσιακές προσεγγίσεις, τα SNN προσφέρουν βελτιωμένη αποδοτικότητα και αποτελεσματικότητα στην επεξεργασία πολύπλοκων συνόλων δεδομένων.

Οι περιορισμοί των παλαιών τρανζίστορ κατά την εφαρμογή σύγχρονων αλγορίθμων μηχανικής μάθησης έχουν προκαλέσει την έρευνα εναλλακτικών λύσεων υλικού. Η τεχνολογία των λέιζερ έχει εμφανιστεί ως μια πολλά υποσχόμενη υποψήφια λύση, δεδομένης της ενσωματωμένης της συμπεριφοράς των εκρήξεων, παρόμοια με τους βιολογικούς νευρώνες. Επιπλέον, τα λέιζερ προσφέρουν υψηλότερη ταχύτητα και αποδοτικότητα, παρακάμπτοντας ζητήματα όπως η διαρροή ρεύματος και η ανάγκη να φορτίζονται παρασιτικές χωρητικότητες, εξαλείφοντας έτσι το πρόβλημα της απόδοσης. Αυτή η σύγκλιση των αλγορίθμων που εμπνέονται από τη νευροεπιστήμη και της τεχνολογίας των λέιζερ παρουσιάζει μια ελκυστική προοπτική για την προαγωγή των δυνατοτήτων των συστημάτων ΤΝ.

Abstract

This thesis explores the utilization of laser technology for simulating biological neurons and proposes a concept of autaptic memory. With the increasing demand for processing large volumes of data, conventional silicon chips encounter limitations in accommodating machine learning algorithms efficiently. To address this challenge, the research introduces new photonic hardware as an alternative approach.

The methodology is divided into two main parts: firstly, demonstrating the ability of a single laser to exhibit spiking behavior akin to biological neurons, and subsequently, investigating methods to control the output spikes. The second phase involves employing a feedback loop between two lasers, effectively creating a memory system. Various measurements are conducted to analyze the duration and storage capacity of the memory.

The findings affirm the feasibility of using semiconductor optical amplifiers (SOA) to simulate neurons and establish the groundwork for developing a functional memory system. The thesis concludes with insights into the potential of photonics hardware to revolutionize data processing capabilities, offering a glimpse into the future of machine learning-dedicated chips.

In the context of a nascent field, this research contributes essential groundwork for future advancements in hardware design, preparing for the evolving demands of data processing in the digital age.

Keywords: *"Laser technology, Biological neurons, Spiking behavior, Autaptic memory, Photonics hardware, Machine learning, Data processing, Neural simulation, Memory systems, Hardware design, Future technologies, Neuromorphic computing, Silicon chip limitations, Experimental measurements, Neural networks"*

1

Introduction

1.1 The future of AI

Artificial intelligence is currently experiencing rapid growth, with the objective of extending its applications beyond domestic environments, as exemplified by drones, augmented reality, and navigation. Among the crucial considerations, power consumption stands out, necessitating the development of novel algorithms and, more significantly, advanced hardware. Taking inspiration from the human brain, scientists are endeavoring to create a spiking neural network[1], which represents one of the most efficient approaches. This entails transmitting minute pulses between neurons and transistors exhibit inefficiency due to the need for charging parasitic capacities while maintaining a tiny continuous current flow when they are in the cut-off area, resulting in a significant energy inefficiency when considering the scale of a neural network. Simultaneously, neurons establish connections with millions, if not billions, of other neurons, thereby intensifying the fanout problem. This paper presents the utilization of SOA as neuron substitutes under specific conditions, effectively mitigating the fanout problem, elliminating current leakage, and facilitating faster inter-neuron communication.

1.2 Structure

This thesis is structured into six main chapters, each addressing crucial aspects of the research topic. In Chapter 2, the biological foundations of the human brain are explored, delving into the intricacies of neuromorphic machine learning, neuron structures, and modeling techniques. Specifically, the chapter examines the phenomenon of spikes and elucidates neuron dynamics through the lens of dynamical systems theory, with particular focus on the LIF model. Chapter 3 shifts the focus to the fundamentals of light emission, covering topics such as absorption mechanisms, materials properties, and the principles underlying laser operation. A detailed investigation into laser dynamics and behavior is presented in Chapter 4, wherein the laser model is dissected, encompassing concepts such as population inversion, threshold characteristics, and the intriguing analogy between lasers and neurons. Chapter 5 encompasses the experimental measurements conducted to validate the theoretical framework, exploring parameters such as threshold determination, input pulse influence, refractory periods, and firing rates. Finally, in Chapter 6, the concept of autaptic memory is introduced and examined in detail, with discussions on cascatability, input pulse influences, multi-spike phenomena, and the capacity and distance considerations of laser-based memory systems. Through this comprehensive exploration, the thesis aims to contribute to the advancement of photonics-based hardware for machine learning applications.

2

Modeling the human brain

2.1 The human brain

The human brain stands as a remarkable example of intricate networks, recognized as one of the most complex entities known to humanity. It encompasses an estimated 100 billion neurons, along with approximately 100 trillion synapses[i], which account for merely 10% of the total cellular composition within the brain [5]. It is noteworthy that the brain's power consumption remains impressively efficient, with a maximum energy utilization of 25W or a typical daily usage of 10W [4]. To provide a tangible perspective, this energy consumption equates to that of an LED light bulb and on the other hand, there is a growing concern regarding the environmental impact associated with the power consumption of current AI models; hence, the imperative to develop novel technologies for machine learning and artificial intelligence arises.

2.2 Neuromorphic Machine Learning

Neuromorphic machine learning refers to the integration of neuromorphic computing principles and techniques with machine learning algorithms. Neuromorphic computing aims to design and develop computer systems inspired by the architecture and functioning of the human brain's neural networks.

Traditional computing systems, based on the von Neumann architecture[2], have a clear separation between memory and processing units. In contrast, neuromorphic computing systems aim to bring memory and processing closer together, mimicking the parallel and distributed nature of the brain's neural networks. These systems typically employ specialized hardware, such as neuromorphic chips or neuromorphic processors, designed to efficiently perform neural network computations. When applied to machine learning, neuromorphic approaches seek to leverage the unique properties of neuromorphic hardware[3] to enhance the efficiency and performance of learning algorithms. By emulating the brain's neural networks, neuromorphic machine learning models can potentially offer benefits such as improved energy efficiency, faster processing, and the ability to process sensory data in real-time.

Neuromorphic machine learning models often incorporate spiking neural networks (SNNs), which operate based on the concept of spiking neurons that communicate through discrete electrical pulses. SNNs have been shown to be particularly suitable for processing spatiotemporal data and have the potential to achieve high energy efficiency and low latency.

2.3 Neurons

In order to advance in the engineering of neuromorphic machine learning chips, it is crucial to gain a comprehensive understanding of the functionality and mechanisms of neurons. They are the building blocks responsible for transmitting electrical and chemical signals, allowing communication within the nervous system and between the nervous system and other parts of the body. Neurons communicate with each other through synapses. When an electrical impulse (action potential) reaches the axon terminals of a neuron, it triggers the release of neurotransmitters into the synapse. These neurotransmitters then bind to receptor sites on the dendrites or cell body of the next neuron in the pathway, generating a new electrical impulse in that neuron. This process allows for the transmission of information and the coordination of various activities in the body. The classification of neurons encompasses several distinct types, notably sensory and motor neurons[6] . Nevertheless, for the present objective of creating a neuron-like model, we prioritize simplicity, thus not focusing in detail on how each neuron behaves.

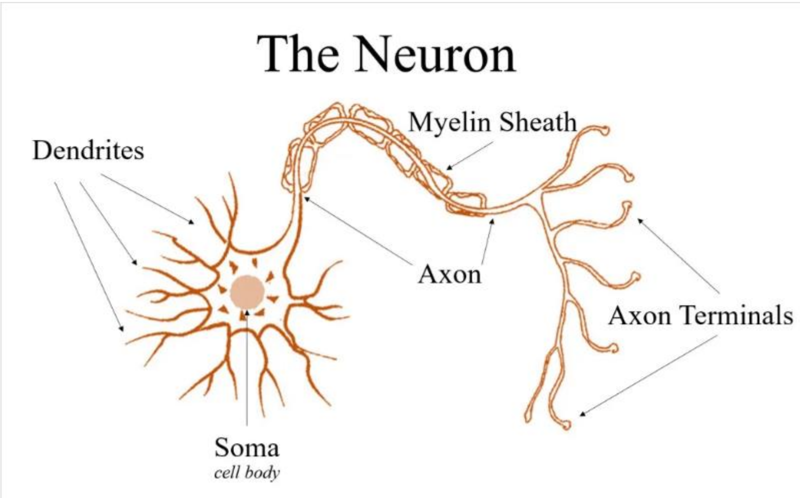

Figure 1: Representaion of a neuron. Teen Brain Talk "Neuron"

2.3.1 Spikes

The soma, or cell body, of a neuron is responsible for integrating incoming signals from the dendrites and initiating the generation of electrical pulses, also known as action potentials or spikes. The process by which the soma generates pulses is a result of changes in the membrane potential[ii]. Each cell has a resting Membrane potential, which is the electrical charge difference across their cell membrane when they are not actively transmitting signals. At rest, the inside of the neuron is more negatively charged compared to the outside, typically around -70 millivolts (mV).

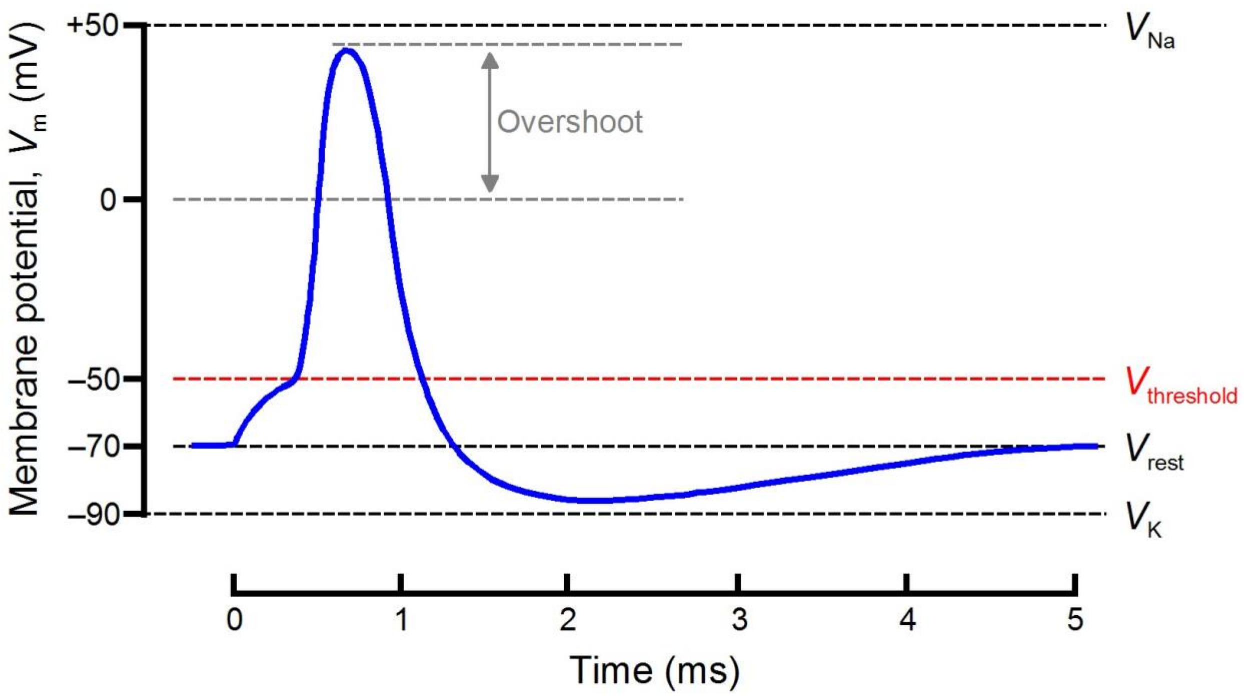

Figure 2: illustrates the concept of membrane potential generating an action potential once it surpasses the threshold level. Image from www.physiologyweb.com

Upon receiving excitatory input from other neurons or sensory receptors, the neuron becomes stimulated. If this stimulation reaches a specific threshold level, a crucial point typically around -55 to -50 millivolts (mV), voltage-gated sodium channels in the cell membrane open. Subsequently, there is a rapid influx of sodium ions into the neuron, leading to a significant depolarization event[7].

As the depolarization progresses, the membrane potential rises towards a positive value. Upon surpassing the threshold, an all-or-nothing response known as an action potential is triggered. During the action potential, the membrane potential experiences a rapid and substantial depolarization, reaching approximately +40 mV. At this stage, voltage-gated potassium channels open, enabling potassium ions to leave the neuron, initiating the repolarization or reset phase.

It is important to note that once the action potential is triggered, it propagates along the neuron's axon, allowing the rapid transmission of signals to communicate with other neurons or effector cells within the nervous system. The mechanism depicted in Figure 2 underlies the fundamental process by which neurons process and transmit information in the nervous system.

2.3.2 Neuron Modeling

Given the intricate nature of neurons, attempting to employ static equations to address their complexities would be an exceedingly challenging task. Nevertheless, by formulating the neuron as a dynamical system, the intricacy of the problem becomes notably more manageable. Dynamical systems, with their capacity to integrate time-dependent variables and consider the evolving states over time, offer a more suitable and efficient approach to describe the behavior of a neuron. By capturing the dynamic interactions and temporal evolution of various neuron parameters, a dynamical systems framework facilitates a deeper understanding and analysis of neural activities without becoming entangled in the overwhelming complexity posed by static equations.

Over the course of years, numerous models have been developed to describe neurons within the context of spiking neural networks (SNNs). This arises from the profound trade-off between attaining biological plausibility and enabling swift computational processing. While the Hodgkin-Huxley(HH)[7] model meticulously captures the intricacies of neuron biology, implementing it in large-scale SNNs necessitates immense computational resources.

Extensive studies exploring neuron morphology and physiology have yielded insights that the Leaky-Integrate-and-Fire (LIF) model emulates a diverse array of observed biological phenomena while remaining amenable to realistic computational demands for large-scale SNNs. The LIF model provides a more simplified and computationally efficient representation of neuron behavior, making it particularly appealing for simulating vast neural networks.

2.4 Dynamical Systems

The equations derive from the analysis of the neuron as a dynamical system, they constitute a fundamental mathematical framework for describing the behavior and evolution of various systems over time. A dynamical system is characterized by three key components: state variables, time and dynamics. Each state represents a system’s condition. Time serves as the independent variable, capturing the system's evolution over a continuous or discrete temporal domain. Dynamics, or the evolution rule, specifies the mathematical relationships governing the interplay of state variables and their changes over time. Dynamical systems theory is a powerful tool used in various fields such as physics, engineering, biology, economics, and chaos theory. It helps in understanding and predicting the behavior of complex systems and plays a significant role in modeling and simulating real-world phenomena. Before analyzing neurons and lasers, a simple example of a dynamical analysis is presented.

2.4.1 Pendulum as a dynamical system

The pendulum's oscillatory motion is among the most iconic and instructive demonstrations of employing differential equations and phase portraits to characterize its dynamics over time. Its ubiquity in daily life and the simplicity of its underlying mechanics makes it an ideal exemplary for illustrating the principles of dynamical systems analysis. The oscillation can be described using a second-order linear differential equation[iii], which relates the angular displacement and velocity of the pendulum with respect to time. This equation derives from the fundamental principles of classical mechanics and assumes small-amplitude oscillations.

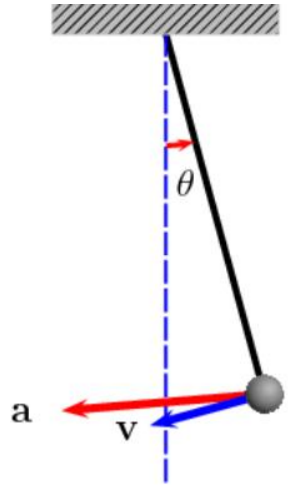

Figure 3: pendulum in motion with arrows denoting position and velocity. Source: Wikipedia

At any given time, the system possesses a variable θ denoting the angular displacement of the pendulum from its equilibrium position. Thus, θ serves as one of the state variables characterizing the system's configuration.

In addition to θ, the system exhibits another state variable, V, representing the velocity of the weight (or pendulum bob). The velocity of the weight, denoted as V, can be expressed as the angular velocity of θ, denoted as θ', which arises from the correlation between the angular displacement and the sine of θ as well as the length of the string.

Mathematically, the relationship can be represented as follows:

$$V = L\frac{d\theta}{dt}\,sin\theta$$ **Equation 2.1**

To predict the forthcoming state of the system, it necessitates the angular acceleration, denoted as θ”,[iv] in addition to the angular displacement. Hence, the state of the system at any specific time is contingent on two variables, θ and θ’’, which will be the state variables. To come up with the equations that govern the system, finally an equation that describes the angular acceleration based on the displacement is needed. Which can simply be found by using the first derivative of the equation 2.1:

$$\ddot{\theta} = -\frac{g}{L}\sin\theta(t) \qquad \textbf{Equation 2.2}$$

At this point, we have the system variables and the system’s equations, thus we can procced at creating a phase portrait

A phase portrait is a graphical representation of the state space of a dynamical system, illustrating the evolution of the system over time. In the context of a simple pendulum, the phase portrait typically displays the relationship between the angular position (θ) and the angular velocity (ω) of the pendulum.

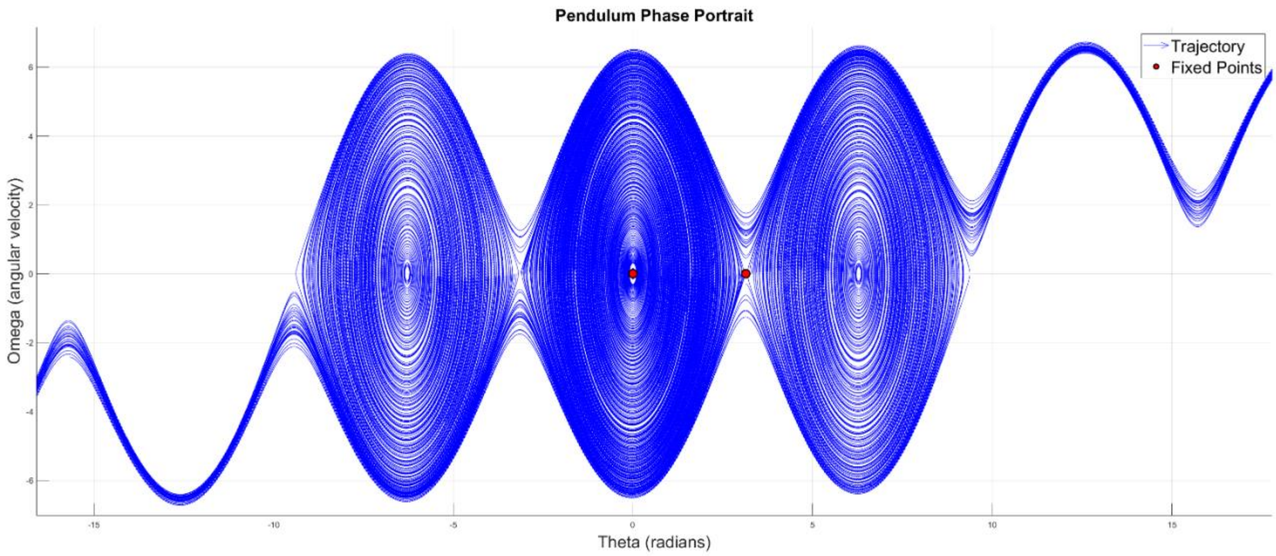

Figure 4: illustrates the phase portrait of a pendulum, a graphical representation showcasing the evolution of the system in its dynamical state space. Fixed points situated at θ=0 and θ=π, also known as the hanging and upright positions. The upright position is characterized as a repeller, as minuscule perturbations will set the pendulum in motion, whereas the point at θ=0 is classified as an attractor, signifying the pendulum's inexorable return to this position over an infinite amount of time.

In the context of a dynamical system, fixed points, also known as equilibrium points or steady states, are positions in the phase space where the system's state remains constant over time. Mathematically, a fixed point occurs when the derivatives of the system's state variables with respect to time are equal to zero. In other words, the system is in a state where there is no change. Fixed point can be divided into 3 categories:

Stable Fixed Point **(Attractor):** In the vicinity of a stable fixed point, trajectories tend to converge towards the fixed point over time. Small perturbations or disturbances lead the system back to the fixed point, indicating stability. In a phase portrait, a stable fixed point is often represented by a point attractor.

Unstable Fixed Point (Repeller): Near an unstable fixed point, trajectories diverge away from the fixed point over time. Small perturbations or disturbances result in trajectories moving away from the fixed point, indicating instability. In a phase portrait, an unstable fixed point is often associated with a repeller.

Saddle Point: A saddle point is a fixed point with both stable and unstable directions. Trajectories approaching the saddle point along one direction are attracted (stable), while trajectories moving away along another direction are repelled (unstable). Saddle points are characterized by a combination of stability and instability.

2.5 LIF Model

In the realm of computational neuroscience, the Leaky Integrate-and-Fire (LIF) neuron model serves as a foundational concept, providing a simplified yet insightful representation of neuronal behavior. This introductory chapter aims to present an overview of the LIF neuron model, outlining its mathematical framework, dynamic characteristics, and its significance in simulating neural processes.

Understanding the complexity of neural circuits and their information processing capabilities is a formidable challenge. The LIF model, introduced as a computational simplification, allows researchers to dissect and explore the fundamental principles governing neural dynamics. Its efficiency and tractability make it a key player in studying both individual neurons and large-scale neural networks.

The core of the LIF neuron model lies in its mathematical formulation. The model is characterized by ordinary differential equations governing the evolution of the membrane potential over time. Key parameters, such as the membrane time constant (τ_m), threshold potential (V_{th}) and reset potential (V_{reset}), collectively define the model's behavior. A more mathematical representation of the model is as follows[10]:

$$V_m' = \frac{V_L}{\tau_m} - \frac{V_m(t)}{\tau_m} + \frac{1}{C_m} I_{app}(t) \qquad \begin{cases} if\ V_m(t) > V_{threshold} \\ then\ fire\ and\ V_m(t) = V_{reset} \end{cases} \qquad \textbf{Equation 2.3}$$

Where $V_m(t)$ is the rate of change of the membrane potential V_L / τ_m is the active pumping, $V_m(t)/ \tau_m$ describes the leakage and $1/C_m * I_{app}(t)$ adds the external spikes.

The manifestation of spike events in the context of the Leaky Integrate-and-Fire (LIF) neuron model is succinctly captured through the imposition of a Dirac delta function, denoted as $\delta(t - t_j)$ where t_j signifies the temporal delay associated with the spike occurrence.

The temporal dynamics of the LIF neuron's membrane potential reveal a distinctive spiking behavior. As the membrane potential integrates synaptic inputs, it undergoes a gradual increase until reaching a predefined threshold. The ensuing spike event involves a rapid reset of the membrane potential to a resting state, capturing the essence of action potential generation.

3

Photonics

As previously elucidated, the resolution to the fanout problem and the optimization of energy efficiency are achieved through the utilization of light. However, a comprehensive understanding of the fundamental principles of light is imperative to facilitate the implementation of the laser in simulating neuronal behavior. Delving into the intricacies of the laser, this section will elucidate its key attributes and operational characteristics. While the physics of light is a broad domain, we will concentrate solely on aspects directly pertinent to our specific implementation, streamlining the discourse for a more focused examination of the laser's role in the experiment.

3.1 Light Emission

Electrons within atoms exhibit quantized energy levels which are distinct and defined, corresponding to specific orbits or shells within the atom. The electron transitions between these energy levels are governed by the principles of quantum mechanics.

An electron typically occupies the lowest energy level, referred to as the ground state (band E_1), but can absorb energy and transition to a higher energy level, known as the excited state (band E). This absorption of energy can occur through various mechanisms, such as exposure to external light or electrical stimulation. Once in the excited state, the electron is in an unstable configuration and tends to return to its lower energy state.

When the electron transitions back to the lower energy level, it releases the excess energy in the form of a photon. The energy of the photon is directly proportional to the energy difference between the excited and

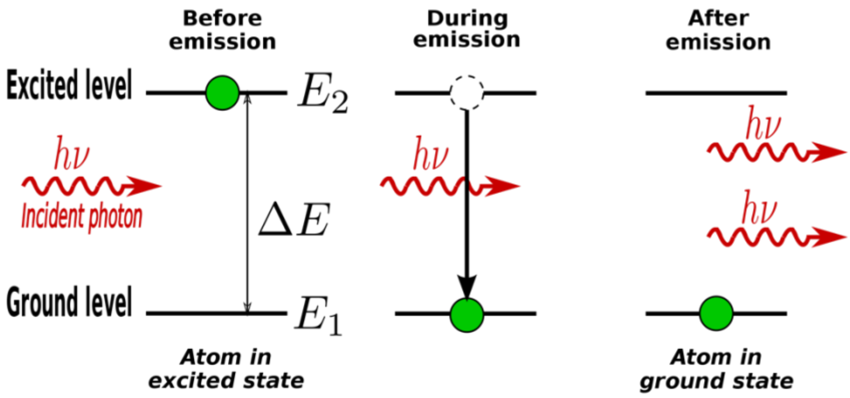

Figure 5: illustrates a fundamental interaction within a quantum cavity system, showcasing the intricate dynamics between photons and electrons. In the scene, a photon, represented by a distinct burst of radiant energy, is captured at the precise moment of entry into the cavity. Within this confined space, it engages with an electron, extracting energy from its quantum state through a process known as energy transfer. Remarkably, this interaction catalyzes the creation of a duplicate photon, mirroring the original with identical properties. Such phenomena exemplify the profound principles of quantum mechanics, where particles exhibit both wave-like and particle-like behaviors, underscoring the delicate interplay between light and matter at the quantum level. This image serves as a visual testament to the fascinating phenomena occurring within quantum cavities and the intricate dance between photons and electrons that underpins their behavior. Image was take from Wikipedia.

ground states. Consequently, photons emitted during this process exhibit specific wavelengths, corresponding to different regions of the electromagnetic spectrum. Moreover, the material composition plays a crucial role in determining the energy levels and the emitted photons' characteristics. For instance, different elements and compounds have unique energy level structures, resulting in the emission of photons with distinct colors and wavelengths.

An alternative method for light generation resides in stimulated emission, a process characterized by the induction of electrons to higher energy levels through current injection. In this paradigm, electrons are elevated to higher energy states, and upon descent to lower levels, photons are emitted within a resonant cavity. Significantly, stimulated emission embodies a distinctive feature: photons discharged during this process possess identical characteristics to their precursors. This phenomenon is a consequence of the coerced energy transfer from electrons to photons, resulting in a cascade of emissions featuring photons with precise attributes. Stimulated emission serves as a cornerstone in the development of lasers, amplifying coherent light by harnessing the principles of quantum optics and electron-photon interactions. This intricate process underscores the sophisticated interplay between electron dynamics and photon generation, contributing to advancements in optical technologies.

3.1.1 Absorption

Conversely, in a reciprocal manifestation of optical processes, electrons possess the ability to absorb energy from photons traversing through the cavity. This phenomenon, aptly termed absorption, involves the transfer of energy to electrons, propelling them to higher energy states. The crux of absorption lies in the intricate interaction between photons and electrons, where the latter harness energy from the incident photons, facilitating an elevation to higher energy levels within the atomic structure. Notably, absorption serves as the cornerstone mechanism harnessed in solar panels, wherein incident photons from sunlight are absorbed within the photovoltaic material. This absorption-induced energy transfer initiates a cascade of events that culminate in the generation of an electric current, underscoring the pivotal role of absorption in the conversion of solar energy into electrical power.

3.1.2 Material

But why doesn't your phone, TV remote or even cables emit light? The answer is material. Modern electronic systems predominantly employ silicon semiconductors, a material acknowledged for its suboptimal light-emitting characteristics. This inadequacy can be attributed to the positioning of energy levels within silicon, specifically delineated by the concept of bandgaps.

Within the realm of bandgap classifications, two fundamental categories emerge: direct and indirect. In a direct bandgap semiconductor, the minimal energy requisite for an electron to traverse from the valence

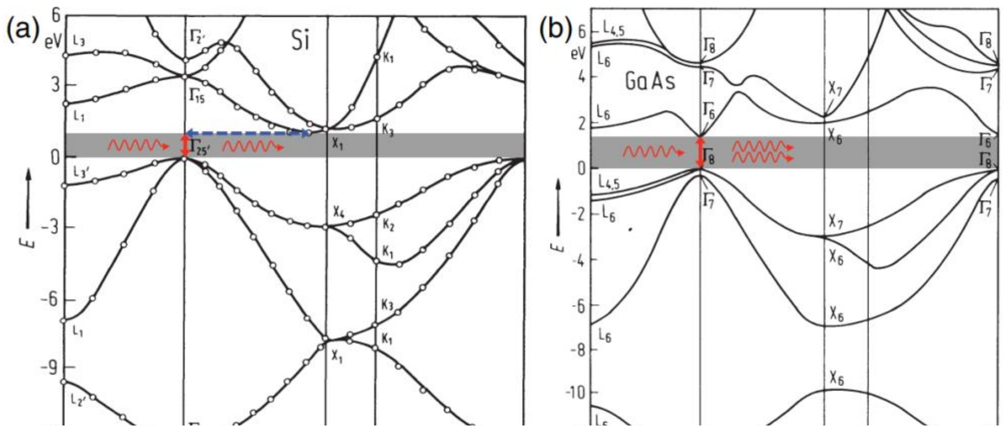

Figure 6: In image a, representing indirect bandgaps, the energy states of electrons and holes do not align neatly, leading to a less efficient production of photons. Conversely, in image b, the bands align more closely, facilitating the generation of photons with greater ease. Adapted from Neuromorphic engineering

band to the conduction band, denoted as the bandgap, aligns precisely with a specific momentum. This alignment facilitates a highly efficient transition, wherein both energy and momentum are conserved. Consequently, semiconductors characterized by a direct bandgap, such as gallium, demonstrate enhanced efficacy in the emission of photons. Conversely, within the domain of indirect bandgap semiconductors exemplified by silicon, a discordance arises in the momentum of electrons transitioning between the conduction and valence bands. This misalignment renders the transition less efficient in terms of momentum conservation. Consequently, silicon exhibits a diminished effectiveness in directly emitting photons from band-to-band transitions. The surplus energy incurred during these transitions tends to dissipate predominantly in the form of heat, rather than the desired emission of light.

In a broader context, materials falling within the IV-VI and III-V groups are distinguished by their manifestation of direct bandgaps, endowing them with the capacity for light emission while materials beyond this classification generally lack this intrinsic ability.

3.2 The Laser

Light Amplification by Stimulated Emission of Radiation (L.A.S.E.R), distinguish themselves through a comprehensive set of characteristics that set them apart from conventional light sources. Notably, the concept of a lasing threshold is fundamental to lasers (will be further explained in chapter 4), representing the minimum level of pump power or optical intensity required to initiate and sustain laser action. Laser light's remarkable coherence extends beyond being merely spatial and temporal; it is characterized by exceptionally high coherence lengths, enabling the propagation of well-defined wavefronts over considerable distances. This coherence is further manifested in the monochromatic nature of laser light, where the emission spectrum is exceedingly narrow, resulting in a singular, well-defined wavelength—a property particularly advantageous in applications demanding precision and spectral purity. Moreover, lasers exhibit extraordinary directionality, allowing for the generation of tightly focused beams, a feature harnessed in diverse applications ranging from medical procedures to cutting-edge technologies. The intense concentration of laser beams, often several orders of magnitude higher than that of conventional light sources, underpins their effectiveness in tasks such as materials processing and telecommunications. Furthermore, the stability of laser output, characterized by minimal fluctuations in power and wavelength, reinforces their utility in scientific research and industrial applications where consistency is paramount. These multifaceted characteristics collectively underscore the versatility and significance of lasers across a broad spectrum of scientific, technological, and industrial domains.

3.2.1 Optical Resonators

Optical resonators, also known as optical cavities, are fundamental components in laser systems and optical devices. They play a crucial role in enhancing the coherence and intensity of light by confining it within a specific spatial region. This confinement allows for the amplification of specific wavelengths through the process of stimulated emission. A typical optical resonator consists of two mirrors facing each other; one mirror is highly reflective, while the other may be partially transmissive, allowing a portion of the light to exit the cavity. The mirrors create an optical feedback loop, leading to the constructive interference of light. There are mainly three types or resonators, *Fabry-Perot, Ring Resonator and Microresonators*[9]. In this section the focus will be on Fabry-Perot, since they are mainly the ones used in lasers.

3.2.2 Fabry-Perot Resonator

The Fabry-Perot resonator constitutes a crucial optical cavity formed by two parallel mirrors, prominently reflective and partially transmissive. Named after Charles Fabry and Alfred Perot, this resonator serves as a foundational element in various optical systems, including lasers, filters, and spectrometers. Its core architecture involves two mirrors, one possessing nearly complete reflectivity and the other designed for partial transmission, thereby establishing an optical cavity.

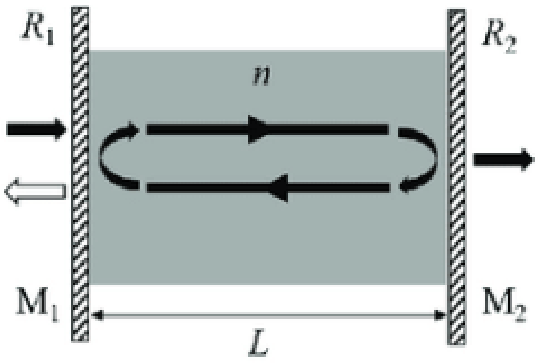

Figure 7: Schematic of a Fabry-Perot resonator consisting of parallel mirrors M 1 and M 2 with reflectances of R 1 and R 2 , respectively, surrounding a cavity medium of refractive index n and thickness L. Light introduced from one side undergoes multiple reflections, leading to partial transmission from the other side. Bitarafan, Mohammad & DeCorby, Ray. (2017). On-Chip High-Finesse Fabry-Perot Microcavities for Optical Sensing and Quantum Information. Sensors (Basel, Switzerland). 17. 10.3390/s17081748.

Within this cavity, light undergoes multiple reflections, resulting in constructive interference under specific resonance conditions. The performance of the Fabry-Perot resonator is intricately linked to the reflective coatings on its mirrors. One mirror is engineered for nearly 100% reflectivity, while the other is selectively transmissive. These coatings, meticulously tailored for optimal reflectivity at specific wavelengths, significantly influence the resonator's transmission and reflection characteristics. The partially transmissive mirror facilitates the transmission of a specific fraction of incident light, constituting the resonator's output or transmission. This dual capability, reflecting light between mirrors and permitting transmission, renders the Fabry-Perot resonator versatile across various optical applications within scientific and industrial domains.

In the dynamic interplay within the laser cavity, the traversing photons engage in collisions, manifesting as pivotal events shaping the optical characteristics of the laser system. In instances where photons exhibit congruent phases, constructive interference ensues, resulting in a pronounced doubling of their amplitude. Conversely, encounters with photons characterized by a phase difference of π lead to destructive interference, attenuating the overall amplitude. These interference phenomena critically influence the emergent optical output of the laser. Upon plotting the laser output in a two-dimensional graph, juxtaposing amplitude against frequency, a discernible pattern emerges. Remarkably, the graph unveils a selective frequency transmission profile, underscoring the laser's propensity to selectively amplify and emit specific frequencies. This intricate interplay of phase coherence and interference underscores the nuanced behavior of the laser system, elucidating the intricate dynamics governing its spectral output. Further exploration and understanding of these phenomena contribute to the refinement of laser technologies and their diverse applications in fields ranging from telecommunications to materials processing.

3.2.3 Phase Shift

In our earlier discussion, we briefly overlooked the intricate mechanisms underlying the occurrence of phase shifts in photons within a laser cavity, emphasizing the role of stimulated emission in maintaining identical characteristics between incident and generated photons. However, an intriguing question persists: why do they not invariably exhibit identical phases? The unequivocal response to this query is that, indeed, they do. Yet, as photons traverse the laser cavity, their trajectory becomes punctuated by a myriad of interactions, chief among them being collisions with other particles and reflections from mirrors. These encounters introduce nuanced phase shifts to the photons, shaping their ultimate behavior. Furthermore, the intrinsic properties of the gain medium, such as its refractive index, play a contributory role in dictating phase alterations. An additional pivotal determinant of phase shifts is the length of the cavity itself. The progression of a wave within the cavity can coincide with the completion of an entire oscillation period upon striking a mirror. However, envisioning the mirror positioned at a minutely altered distance introduces a dynamic wherein photon reflection may transpire before the completion of one oscillation, or conversely, post-oscillation. This intricate interplay between inherent properties and cavity dynamics elucidates the multifaceted nature of phase shifts in the laser system.

Mathematically, to ascertain the conditions for lasing within a Fabry-Perot (FP) laser, the phase of a photon must adhere to the following equation:

$$\varphi = 2\kappa\pi \qquad \kappa \in \mathbb{Z}$$ **Equation 3.1**

$$Where: \varphi = \frac{2\pi\eta L}{\lambda} = \frac{\omega\eta L}{c}$$ **Equation 3.2**

Where L is the distance between the two mirrors, λ is the vacuum wavelength, η the refraction index.

3.3 *Relaxation Oscillations*

The occurrence of relaxation oscillations during the initiation of lasing in a laser system can be attributed to the intricate interplay between gain, losses, and the cavity dynamics. In the initial phases, the gain medium of the laser, driven by an external pump or excitation source, begins amplifying photons. However, during this startup process, the gain and loss mechanisms within the laser cavity are not instantaneously balanced. The transient imbalance leads to periodic variations in the net gain and loss, resulting in oscillatory behavior in the output power. These oscillations signify the laser system's dynamic attempt to establish equilibrium, as it navigates through phases of amplification and relaxation. The interplay of parameters such as the gain medium characteristics, cavity design, and the interplay of photons with mirrors contributes to the nuanced oscillatory response. As the laser system progresses, these transient oscillations gradually subside, giving way to a stabilized, continuous lasing state as the gain, losses, and cavity properties reach an equilibrium. Understanding and characterizing these relaxation oscillations are pivotal for optimizing laser performance and ensuring a reliable and predictable output.

In the subsequent chapter, the utilization, and criticality, of the observed phenomenon are demonstrated in the simulation of a neuron using a laser.

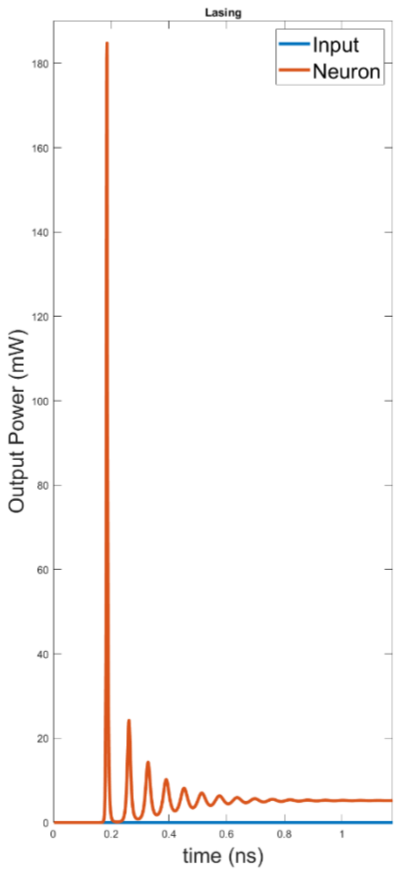

Figure 8: A temporal representation, or timetrace, of the power output of a laser, revealing the characteristic period of relaxation oscillations.

4

Simulation

The subsequent section delineates the mathematical model employed for the laser and repetitive simulations conducted on MATLAB to facilitate the generation of pertinent graphs and enhance comprehension of laser dynamics. Notably, parameters intrinsic to the model and external factors, such as pulse width, delay, and peak power, are systematically adjusted throughout the investigation. This iterative process aims to devise an optimal configuration conducive to fulfilling the neuronal requirements essential for encoding when integrated into a system.

4.1 The Laser Model

In the following research model, a quantum well (QW) laser is employed, adhering to the foundational principles of population dynamics, stimulated emission, and absorption akin to traditional laser models. Nonetheless, the utilization of the quantum well model imparts distinct advantages over the Fabry-Perot (FP) laser model, offering attributes that are not attainable through the implementation of the FP configuration.

Initially, the incorporation of quantum wells, which are thin semiconductor layers confining charge carriers vertically, is observed to augment the likelihood of carrier recombination, thereby yielding heightened emission efficiency. Furthermore, they often manifest lower threshold current densities, and narrower linewidths, attributes attributable to the quantum confinement effect. In the pursuit of establishing an interconnected network of these lasers, considerations encompass the imperative of achieving high communication speeds between neurons. Such a requisition is notably addressed by quantum well lasers, simultaneously offering lower energy consumption, due to their lower lasing thresholds. Lastly, it is noteworthy that semiconductor (SW) lasers, by virtue of their reduced sensitivity to temperature fluctuations, emerge as an advantageous choice for deployment within extensive network configurations.

4.2 Population Inversion

Population inversion is a crucial phenomenon in lasers, occurring when more atoms or molecules exist in higher energy states than in lower ones. In the context of lasers, this inversion of the typical population distribution sets the stage for stimulated emission, a key process in laser operation. Stimulated emission involves the release of photons from atoms or molecules that are already in an excited state, triggered by the presence of incident photons with the same energy. This creates a cascade effect, leading to the emission of coherent and collimated light – the laser beam. Population inversion is essential for laser action because it establishes the conditions for amplification and sustained emission of light, forming the basis for the coherence and directionality characteristic of laser beams.

4.3 Threshold

The concept of population inversion is intimately connected to the threshold in laser operation. The threshold in a laser refers to the minimum level of population inversion required to achieve and sustain laser action. Below this threshold, the spontaneous emission of photons predominates, leading to a non-coherent output. However, once the population inversion surpasses the threshold, stimulated emission begins to dominate, resulting in coherent and amplified light output in the form of a laser beam. Achieving and maintaining a population inversion above the threshold is essential for the sustained and efficient operation of a laser, ensuring that the amplification of light through stimulated emission consistently outweighs losses and spontaneous emission. Therefore, population inversion serves as a critical condition for surpassing the threshold and enabling the coherent and directional emission of light.

4.4 Current Injection

Utilizing injection current in a laser system enables precise control over the population inversion, allowing the laser to operate in proximity to the threshold. Analogous to the membrane potential in a neuron, the injection current serves as a modulating factor influencing the energy states of the active medium in the laser. By adjusting the injection current, the population inversion can be finely tuned, ensuring that the laser hovers near the threshold level. This control mechanism is akin to regulating the membrane potential in a neuron to modulate its excitability. In both cases, maintaining a specific condition—whether it's proximity to the threshold in lasers or a specific potential in neurons—facilitates optimal performance. This parallel underscores the utility of injection current as a means of controlling and stabilizing the laser's operation, much like the regulation of membrane potential in neuronal systems.

4.5 *Laser As a Neuron*

The utilization of a laser to emulate a leaky integrate-and-fire (LIF) neuron arises from its inherent resemblance to neuronal mechanisms. This fundamental connection will be elucidated through mathematical analysis in subsequent sections. However, for the current discussion, a more logical approach will be employed to establish the rationale for this simulation.

The threshold, a fundamental attribute of a neuron, plays a pivotal role in determining whether the neuron fires or not. This critical parameter significantly impacts the selection of an appropriate element for simulation. As previously mentioned, the inherent lasing threshold of a laser renders it an ideal candidate for emulating neuronal dynamics. This resemblance between neuronal and laser thresholds stems from their shared ability to transition between distinct states in response to external stimuli.

The excitation of electrons via current injection mirrors the functionality of membrane potential in neurons; this analogy highlights the fundamental mechanisms shared. The injection of current serves to maintain the laser in a state of heightened excitability, priming it to respond to external stimuli. Upon receiving sufficient external input, the laser's current surpasses the lasing threshold, triggering a sharp increase in its output intensity, analogous to a neuronal action potential.

To accurately simulate neuronal dynamics, a reset mechanism is indispensable. Upon cessation of external stimuli, electrons in the higher energy band gradually relinquish their energy to photons, causing the laser's current to recede to the level of the injection current. This natural decay effectively resets the laser's state, mimicking the refractory period observed in neurons. The natural decay of the laser's excited state serves as a *passive reset mechanism*, returning the laser to its ground state after emitting a light pulse

The passive reset has the drawback of creating wider pulses, however an active reset mechanism can be engineered by the use of an external signal to quickly quench the laser's population inversion. This can be done by applying a negative voltage to a saturable absorber, which is a material that changes its optical properties when it is illuminated with light[11].

4.5.1 *Analytical approach*

Without delving extensively into the mathematical underpinnings, a compelling argument for the potential efficacy of lasers in emulating neuronal behavior lies in the remarkable similarity between the equations governing the Leaky Integrate-and-Fire (LIF) model and the gain dynamics observed in Semiconductor Optical Amplifiers (SOAs) under short input pulses. This congruence offers a persuasive rationale for considering lasers as viable candidates for neural simulation.

$$\underbrace{\frac{\mathrm{d}N'(t)}{\mathrm{d}t}}_{\text{Activation}} = \underbrace{\frac{N'_{\text{rest}}}{\tau_e}}_{\text{Active pumping}} - \underbrace{\frac{N'(t)}{\tau_e}}_{\text{Leakage}} + \underbrace{\frac{\Gamma a(\lambda)}{E_p} N'(t) P(t)}_{\text{External input}}$$

$$\underbrace{\frac{\mathrm{d}V_m(t)}{\mathrm{d}t}}_{\text{Activation}} = \underbrace{\frac{V_L}{\tau_m}}_{\text{Active pumping}} - \underbrace{\frac{V_m(t)}{\tau_m}}_{\text{Leakage}} + \underbrace{\frac{1}{C_m} I_{app}(t)}_{\text{External input}} .$$

Equation 4.1 Showing the similarity between the LIF Model and the Dynamics of a SOA. Directly refferenced from: Neuromorphic Photonics[10]

5

Measurements

The commencement of measurements is deemed necessary, with the initial step involving the determination of the threshold for each laser. To achieve this objective, various values of injection current are systematically scanned, and the region at which the laser attains a value greater than 0 is approximately identified. Following the attainment of this preliminary approximation, focused investigation within that specific region is subsequently conducted to ascertain the precise value of the threshold.

The subsequent phase involves the measurement of the input current to discern the laser's behavior in response to varied pulses. This process is subdivided into two sequential steps. The first step would be to measure the pulse width and height, followed by the observing the influence of pulse durations on the output.

The investigation into the single neuron chapter proceeds by measuring the laser's capacity to return to its initial state after the cessation of the input pulse, commonly known as the refractory period. This assessment involves the systematic injection of small pulses at progressively shorter intervals. The results demonstrate that the duration of the pulse significantly influences the laser's ability to exhibit multiple spikes.

Subsequently, an analysis of the laser's firing rate is carried out to quantify the speed at which successive spikes are generated. This parameter, akin to neuronal firing rates, offers valuable insights into the temporal dynamics of the laser system. The parallel drawn between the behavior of the laser and the firing patterns observed in biological neurons enhances our understanding of the intricate similarities between these two disparate systems.

5.1 *Finding the Threshold*

In the present laser study, active absorption was employed to enhance the refractory period and induce the generation of narrow spikes. It was observed that varying absorption values led to distinct lasing thresholds, with a direct correlation identified; an increase in absorption corresponded to an elevation in the threshold. This phenomenon can be elucidated by the shortened photon lifetime, necessitating a higher current input to maintain population inversion.

To ascertain the current injection to laser emission, a systematic exploration was conducted by iteratively varying the injection current and observing the resultant number of spikes in the output. Subsequently, the obtained dataset was graphically represented in Figure 9a, illustrating a discernible direct correlation between injection current and output, with the corresponding values subjected to scrutiny. This initial scanning provided an approximate estimation of the threshold. To refine the precision of this determination, a subsequent scan was performed with a finer step size, enabling a more granular assessment to pinpoint the exact threshold value.

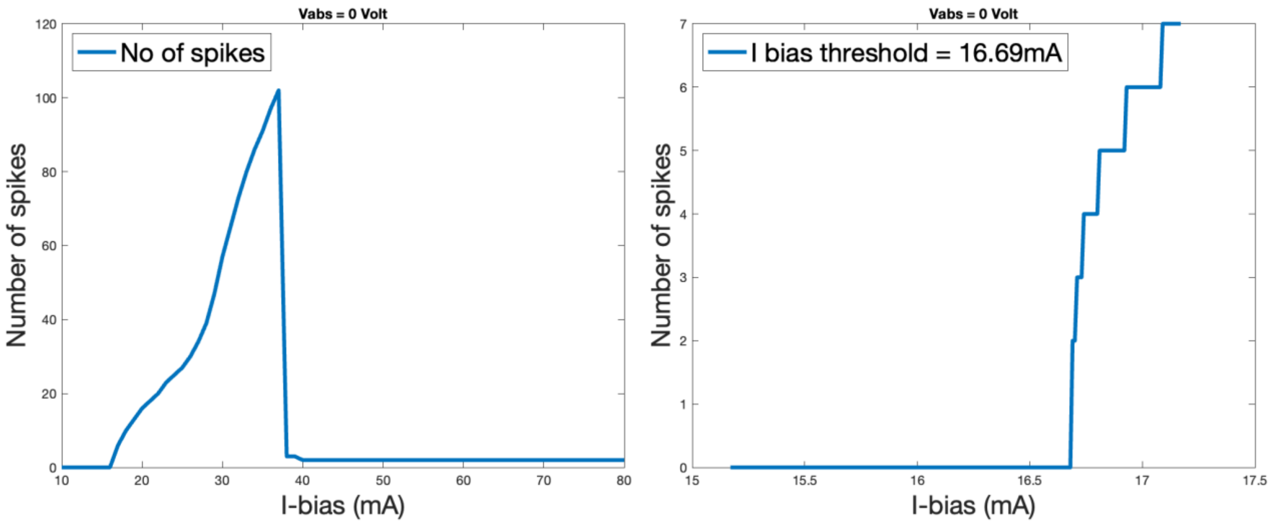

Figure 9: presents a comprehensive depiction of the threshold, with subfigures (a) and (b) providing insights into different scanning approaches. Subfigure (a) illustrates an expansive scanning area, offering an approximate threshold range of 15-18mA under the condition of Absorbers value being equal to 0. In contrast, subfigure (b) employs a finer scanning resolution, characterized by significantly smaller step (x10^{-2}), enhancing the granularity of the threshold exploration.

Employing a parallel methodology across various absorber values, a comprehensive dataset was generated and is presented in the ensuing table. The absorber values ranged from 0 to 5, with corresponding threshold values indicating the requisite current for laser emission. The final injection value, representing the operational current employed throughout the experiment to maintain the laser in a ready-fire state just below the threshold, was determined. This operational value typically stands approximately 0.5 mA below the threshold, allowing for operational flexibility with slight adjustments depending on the specific usage of the laser.

Absorber $(10^{-3}\ Volt)$	Threshold $(10^{-3} Ampere)$	Injection$(10^{-3} Ampere)$
$0\ mV$	$16.69\ mA$	$16.19\ mA$
$1\ mV$	$20.37\ mA$	$19.87\ mA$
$2\ mV$	$24.89\ mA$	$24.39\ mA$
$3\ mV$	$30.44\ mA$	$29.94\ mA$
$4\ mV$	$37.25\ mA$	$36.75\ mA$
$5\ mV$	$45.6\ mA$	$45.1\ mA$

Table 1: correlation between absorber and threshold while calculating an injection value for each different scenario

5.2 Input Influence

Having successfully determined the threshold and established the laser in a ready-fire state, the next phase involves monitoring the output behavior in response to varying inputs. This stage is crucial, given that the ultimate aim of the experiment is to assess the feasibility of incorporating the laser into a neural network, highlighting the significance of controlled pulses. This analytical pursuit is divided into two integral components. Initially, the focus is on attaining a comprehensive understanding of the laser's behavior with respect to the peak power of the input followed by a demonstration on how manipulating the pulse duration serves as a mechanism for controlling the number of spikes generated by the laser.

5.2.1 Peak power

To accurately characterize the relationship between output and input, a methodical approach involves running the model while incrementally increasing the input power and meticulously recording the corresponding output. Subsequently, through a comprehensive analysis of the generated graphs, informed assumptions can be drawn regarding the significance of input power, its behavioral patterns, and whether further exploration is warranted.

As depicted in figure 10, it is evident that the input power does not exert an influence on the total energy of the spike. However, a noteworthy observation lies in the energy distribution. Examination of the initial two graphs reveals a subtle increment in Peak Power as Input Power rises, concomitant with a reduction in pulse width. This discernment leads to the definitive conclusion that the strength of the input does not govern the overall output energy; rather, it orchestrates the manner in which the energy is disseminated. Specifically, heightened peaks correspond to narrower pulses, and conversely. Moreover, it is observed that a cap on the output peak results in a decrease in width.

While input power serves as an influential factor in pulse width modulation, the pivotal determinant for the combination of peak power and width is the strength of the absorber. The direct correlation between absorber strength and injection current logically implies that an increase in absorber strength leads to an overall elevation in output peak power. Thus, the combination of absorber strength and input power emerges as a potent means to exercise precise control over these parameters. The absorber functions as the primary mechanism for determining peak power and width, with minor refinements achieved through adjustments to the input.

It is imperative to consider that a stronger absorber, as elucidated in the preceding section, corresponds to an elevated threshold, thus necessitating a higher input to surpass this threshold. In this context, the injection current values were consistently configured to be 0.5 mA below the threshold. To facilitate laser

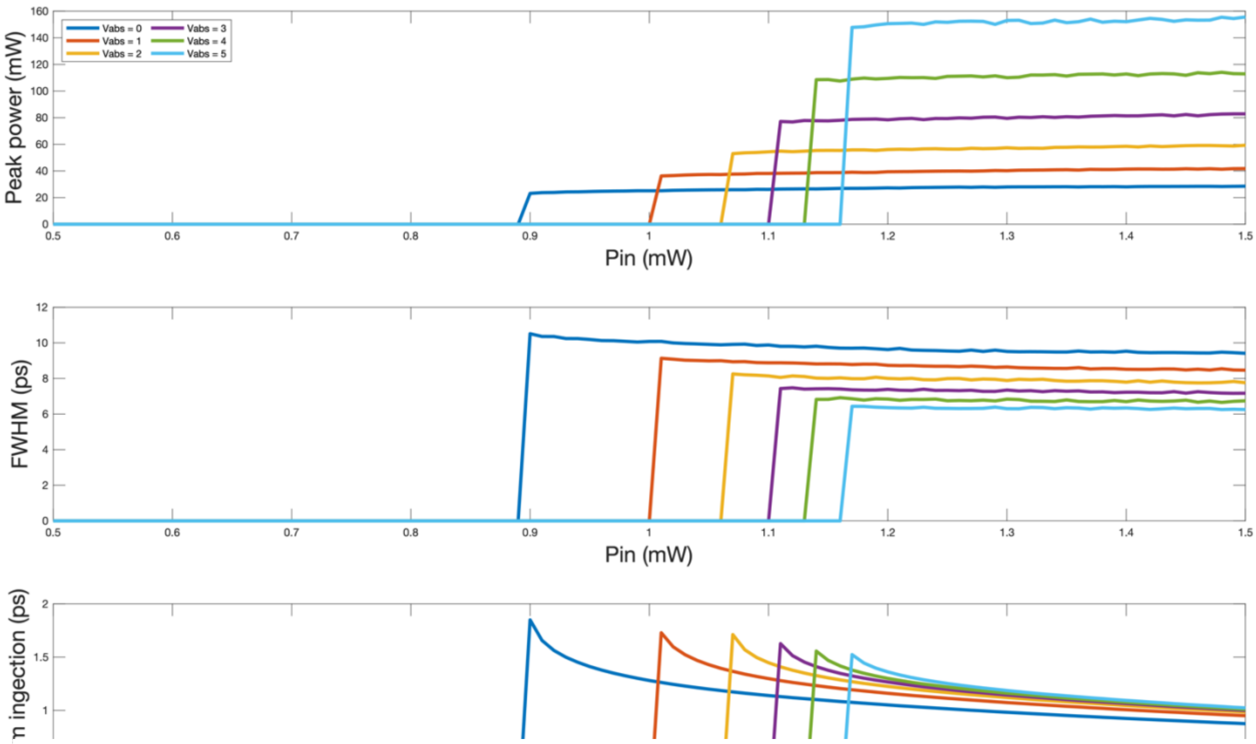

Figure 10: encapsulates measurements derived from the experiment, illustrating the influence of the absorber in conjunction with input power on the control of output strength and width. In Graph (A), a discernible trend is observed, wherein a higher absorber value results in elevated peaks. Additionally, a marginal increase is noted when manipulating the input power. Graph (B) portrays a similar correlation but in relation to pulse width, demonstrating how higher absorber values contribute to narrower pulses, with incremental adjustments achieved through variations in input power. Graph (C) elucidates the relationship between pulse power and the delay from the moment of injection, revealing an exponential increase in delay as input power rises. These observations underscore the nuanced interplay between absorber strength, input power, and their collective impact on the laser's output characteristics.

firing with a smaller input, adjustments in the injection current become imperative, essentially requiring the cumulative sum of injection and input to attain the threshold for successful lasing.

An additional noteworthy parameter, particularly valuable within certain encoding frameworks, is the temporal duration required for the laser to spike following the input reception. As illustrated in figure 10c, there exists an inverse relationship between input power and the time elapsed before the occurrence of the output spike. The exponential rise in delay underscores the significance of operating the laser slightly above the threshold when minimizing delay is a critical consideration.

5.2.2 Pulse Duration

Following a comprehensive investigation into the influence of input amplitude on the dynamic response of the system, attention is now redirected towards the temporal aspects of input pulses and their consequential impact on the system's output. Noteworthy from figure 11 is the observation that an increase in pulse duration corresponds to an escalation in the number of spikes generated by the laser. As demonstrated in a preceding chapter, the laser initiates oscillations in the output before stabilizing to a consistent power output. Due to inadequate input power to sustain prolonged stability, the initial peak of oscillation is observed, followed by a brief hiatus before resurgence. This temporal gap, denoted as the refractory period, will be expounded upon in a subsequent chapter. For the present, the focus is directed toward elucidating how pulse duration contributes to the overall count of spikes.

The measurement process employed to derive the subsequent graphs remains consistent with the preceding one; however, in this instance, rather than incrementing peak power, the pulse width is systematically increased.

A departure from the earlier analysis is evident, as the manipulation of pulse duration no longer exhibits a correlation with the laser's capacity to alter pulse width or peak power, irrespective of the increased energy conveyed by the pulse into the laser. Substantiating this assertion, the ensuing graph provides evidence that both pulse width and peak power persist as constants throughout the scan, with discrepancies in power and width solely contingent upon the absorber's strength.

An additional observation of note pertains to the relationship between increasing voltage at the absorber ends and the output spikes. Notably, when the absorber value is elevated, there is an apparent requirement for an increased input power to facilitate spiking in the laser. However, examination of (a) and (b) graphs reveals a subtle correlation between the two variables. It is important to underscore that this correlation neither conforms to a linear nor an exponential pattern. Moreover, in isolated instances, (ie Vabs = 1 and Vabs = 4), the laser commences firing at identical points. Intriguingly, the emergence of spikes appears to be more closely associated with the refractory period rather than the specific duration of input pulses.

When the absorber's strength remains constant, a discernible pattern emerges: an augmentation in the pulse duration correlates positively with an increased production of spikes. This observation provides valuable insights into the manipulation of input parameters for regulating the quantity of spikes generated from a singular input, particularly considering the typical constancy of absorber values over time.

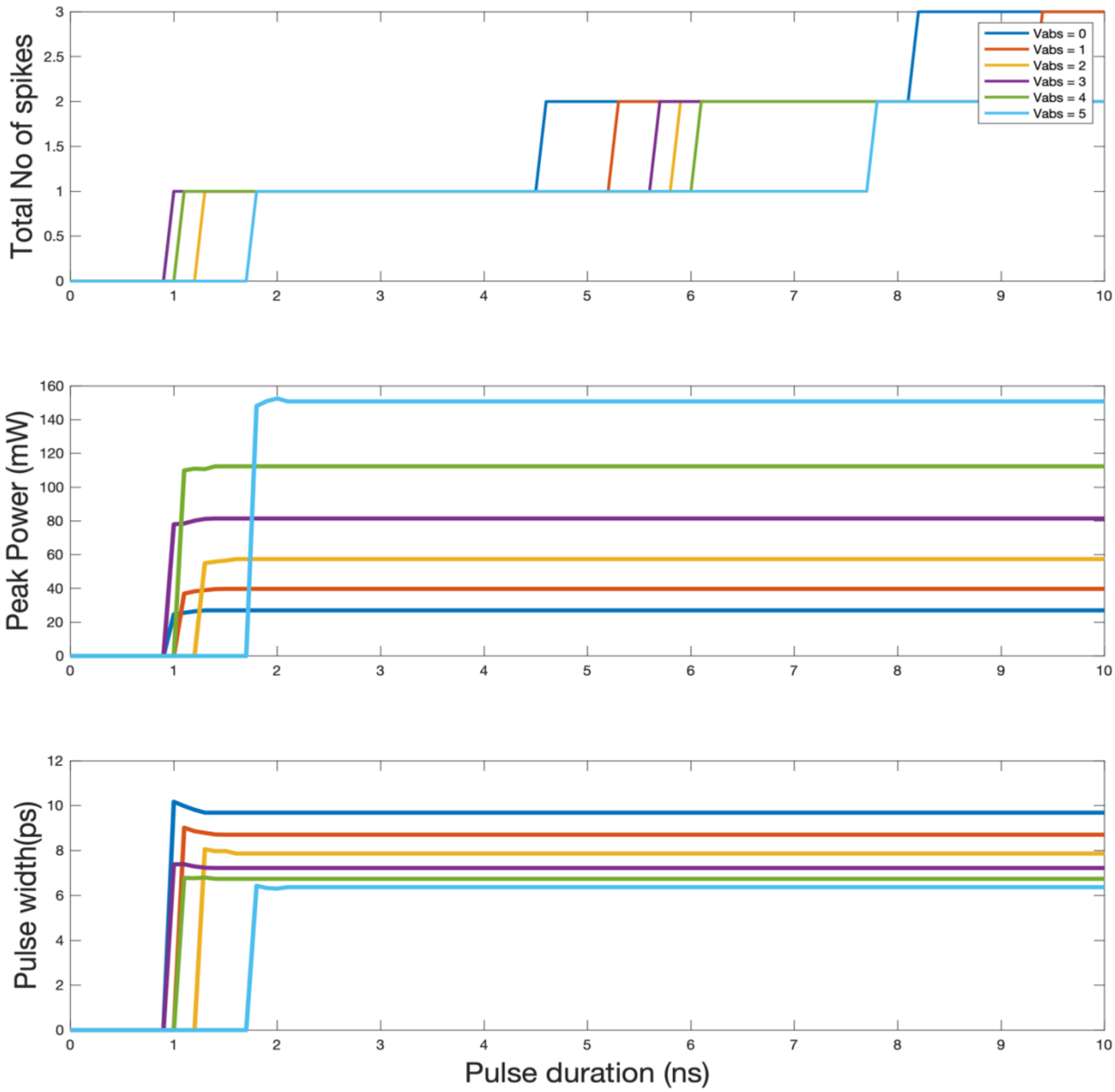

Figure 11: Represents the alike data shown in the previous chapter in the y axes, while tweaking the pulse duration.

5.3 Refractory Period

In biology, the refractory period of a neuron is a critical temporal phenomenon governing the capacity of a neuron to generate action potentials in response to external stimuli. This physiological event consists of two distinct phases: the absolute refractory period and the relative refractory period.

The absolute refractory period is an initial phase immediately following the generation of an action potential, during which the neuron is impervious to any subsequent stimulation. The neuron's ion channels are temporarily inactivated, rendering it refractory to depolarization. Consequently, no stimulus, regardless of intensity, can evoke another action potential during this interval.

Subsequent to the absolute refractory period, the neuron transitions into the relative refractory period. In this stage, the neuron regains partial responsiveness, but the threshold for initiating a new action potential is significantly elevated. While it is not impossible to induce another action potential during the relative refractory period, a more substantial and sustained stimulus is required. The relative refractory period is characterized by increased membrane permeability, particularly to potassium ions, contributing to the heightened threshold.

5.3.1 Reset Mechanism

Given the inherent reset mechanism observed in lasers, characterized by both passive and absorber-driven modalities, it is reasonable to postulate the presence of a refractory period analogous to biological neurons. In essence, the temporal duration required for the laser to return to a stabilized state following activation

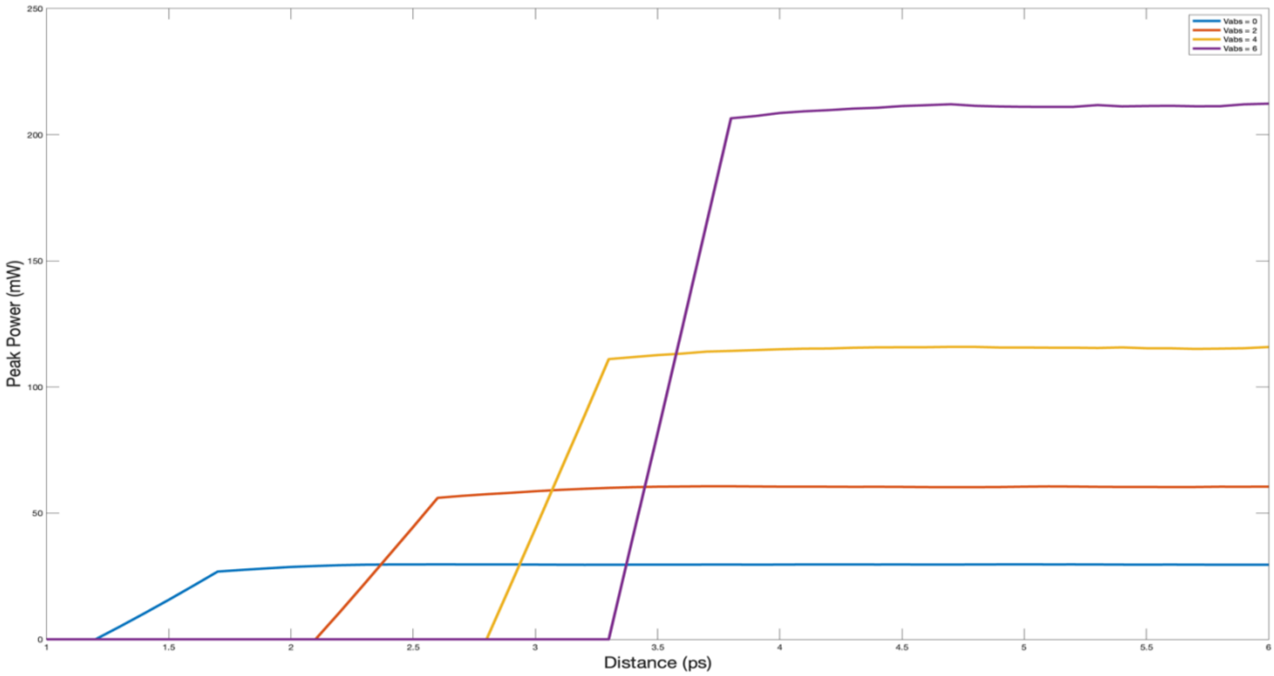

Figure 12: depicts the correlation between peak power and the distance between pulses. The linearly increasing segment of the graph represents the relative refractory period of the neuron, indicating the duration during which a neuron can respond to a stimulus, albeit with diminishing efficiency. The point at which the function transitions from increasing to stable marks the onset of the absolute refractory period, during which the neuron is unable to generate an action potential regardless of the stimulus intensity.

implies a refractory period during which the laser is temporarily incapable of responding to subsequent stimuli. This assertion is grounded in the temporal constraints associated with the laser's transition back to a quiescent state, indicative of a dynamic refractory interval inherent to the laser system.

To procure precise measurements, a consistent laser model was employed, introducing a novel variable to the experimental framework. Termed "distance," this parameter signifies the temporal interval between successive pulses. Systematic modulation of this temporal parameter was undertaken throughout the simulation, involving a gradual reduction in the inter-pulse distance. This methodological approach facilitated the identification of the minimum temporal separation at which the laser ceased to exhibit responsiveness, thereby establishing a tangible metric for the critical refractory period associated with the laser under investigation.

As depicted in Figure 12, the temporal separation between two input stimuli emerges as a pivotal factor influencing the second spike of the laser. Notably, when the inter-pulse distance diminishes to a critical proximity, the laser ceases to manifest any discernible peak. Conversely, an examination of the graph reveals a linear correlation between the distance parameter and the laser's relative refractory period. Prior to reaching its maximum peak power, the laser exhibits an incremental increase in the relative refractory period, illustrated by a linear trend in the graph. Notably, when considering the value of the absorber to be zero, it becomes evident that within the temporal range of 0.5 ps to 1 ps, the laser manifests diminished peaks in comparison to a value such as 2.5ps.

An additional noteworthy observation is the impact of absorber strength on the refractory period. Specifically, an augmentation in absorber strength corresponds to an increase in the refractory period. This relationship is logically coherent as the heightened absorber strength directly correlates with the peak power of output pulses, resulting in an extended temporal interval for the laser to return to its resting state.

5.3.2 Time Traces

To elucidate the impact of inter-pulse distance on laser behavior, figure 13 presents time traces of the model. The red line represents the temporal evolution of the laser's output power, while the blue lines depict the input pulses. The initial diagram (5a) strategically employs a minimal pulse distance, significantly below the threshold, showing the laser's response in conditions unfavorable for sustained activation. In contrast, 5b portrays the laser's behavior within the relative refractory period, characterized by a more extended interval between input pulses. Lastly, 5c illustrates a scenario with a substantial temporal gap between pulses, allowing the laser sufficient time to return to a stable state. This comparative representation offers a comprehensive insight into the dynamic responses of the laser model under varying inter-pulse distances.

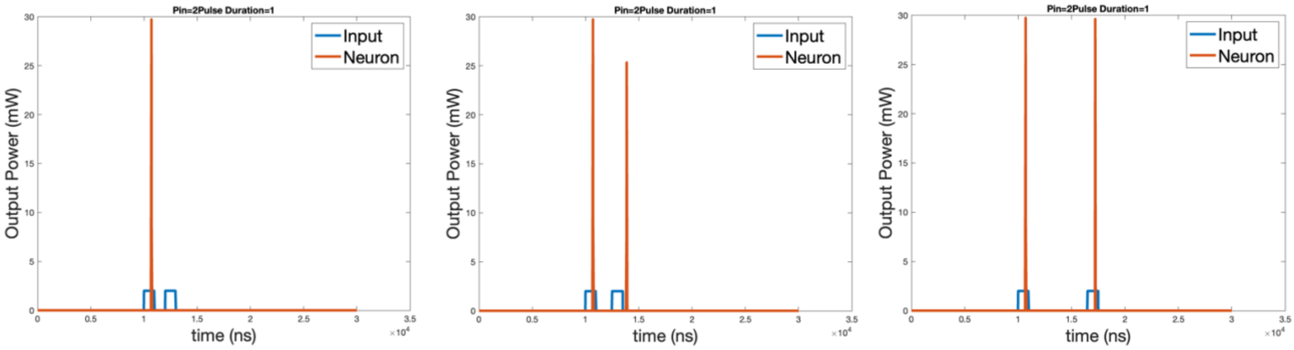

Figure 13: A, B, and C correspond to graphical representations generated through MATLAB simulations, wherein manual adjustments were systematically applied to the pulse distance parameter. These adjustments were made to articulate the laser's behavior under diverse circumstances.

In this phase, it is pertinent to note that the refractory period aligns with the firing rate, a correlation that aligns with logical expectations. However, revisiting Figure 2, we observe that the refractory period occurs only when the membrane potential— or in our case, the population— dips below the relaxation state. When the input power maintains a constant value, the laser seldom dips below the resting state threshold, enabling it to spike more rapidly. This insight underscores the nuanced interplay between input parameters, refractory period dynamics, and the resultant firing rate, contributing to a deeper understanding of the system's behavior.

5.4 Firing Rate

Until this juncture, exploration has been undertaken to assess the influence of input power, pulse duration, and absorber strength on the overall output of the laser. The results have established a positive correlation

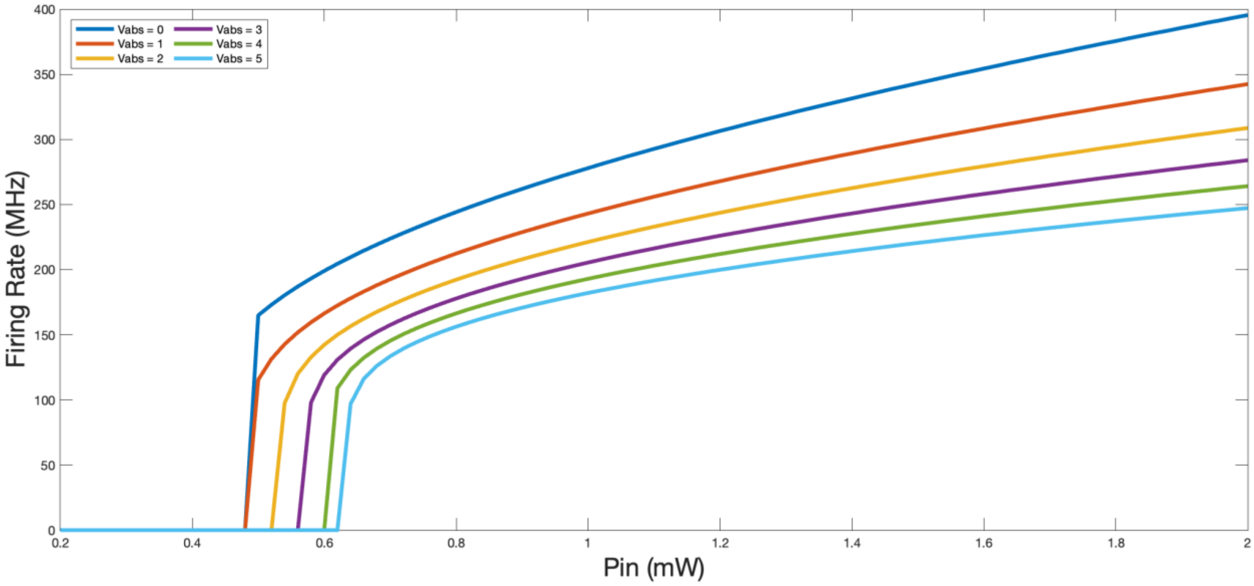

Figure 14: illustrates the linear relationship between the firing rate and the power in the input. Obviously, the firing rate will eventually reach a maximum limit and cease firing thereafter, owing to inherent physical constraints.

between heightened absorber strength and increased output peaks, demonstrated the redistribution of pulse energy through manipulation of input power, and confirmed the induction of consecutive laser firings with extended input durations. Nevertheless, critical inquiries persist: the rate at which the laser spires under prolonged input durations and the manner in which input characteristics affect the firing rate remain unaddressed.

To obtain the most precise data, the measurement methodology involved determining the temporal separation between two consecutive pulses at the commencement, middle, and conclusion stages of the simulation. Subsequently, an averaging process was applied to these measurements, and the derived values were converted into frequencies utilizing the frequency-period relation: $f = T/1$

The graph results indicate that an elevation in input power, concurrent with the ongoing injection of stimuli, augments the firing rate of the laser. This phenomenon can be rationalized by the observation that an increase in power results in narrower pulses. The consequential reduction in pulse width contributes to a shorter reset time, consequently leading to a faster refractory period and, an acceleration in pulse frequency.

6

Autaptic Memory

With a foundational understanding of the behavior of a laser simulating a neuron and the modulatory capacity of the user through manipulations of input parameters, the subsequent phase of exploration in this experiment addresses the prospect of indefinitely retaining a pulse. Given the intrinsic memory capacity of computational systems, the creation of a memoryless chip would render this research futile. A conceivable approach involves the isolation of an optical fiber to form a closed loop, allowing light to perpetually circulate within the loop. The absence of mechanisms for energy dissipation would theoretically enable the pulse to persist indefinitely. However, despite light's remarkable capacity for energy preservation, some energy loss occurs due to refraction. Additionally, dispersion introduces temporal alterations in pulse duration, particularly over extended time periods. In cases where the loop size is constrained, pulse overlap may engender chaotic behaviors, further complicating the pursuit of sustained pulse retention.

The incorporation of two interconnected lasers within a feedback system introduces a viable alternative to the isolated loop concept. In this configuration, the first laser assumes the role of a Master Laser, functioning as the source of the original signal, while the second laser operates as a Slave laser with the primary task of faithfully replicating the provided signal. As elucidated in preceding sections, lasers possess the capability to utilize external light as an excitability mechanism. Consequently, if the Master Laser yields sufficient strength to supply the requisite energy, the Slave laser undergoes excitation, generating an output. Importantly, owing to the intrinsic mechanisms of the laser, the Slave laser not only produces an output but, influenced by its inherent characteristics, regenerates a comparable output mirroring the input—a process tantamount to the regeneration of the initial spike. Subsequently, the output emanating from the Slave laser becomes a feedback signal directed back to the Master Laser, establishing a self-sustaining loop. This recursive process, fueled by the continuous interchange of signals between the Master and Slave lasers, perpetuates indefinitely; thus creating a memory.

6.1 Cascatability

"Cascadability" in the context of neurons generally refers to the ability of neurons to transmit signals or information in a cascade or sequential manner through a neural network. In a neural network, information often flows through multiple layers of interconnected neurons, and the concept of cascading refers to the sequential activation of neurons in response to a stimulus or input.

Neural cascades play a crucial role in information processing and transmission within the nervous system. When a neuron in a neural network is activated, it can transmit signals to connected neurons, leading to a chain reaction of activations. This cascade of activations allows for the integration and processing of complex information as it propagates through the network.

In the initial phase of this experiment, the primary objective was to comprehend the laser as an autonomous entity. Subsequent to this understanding, the integration of the laser into a neural network featuring multiple lasers firing across the layers of the network was undertaken. A pivotal analysis focused on the laser's capacity to stimulate additional lasers, commonly referred to as its cascatability. This examination assumes significance as the cascading behavior of lasers is instrumental in the functionality of a neural network. Furthermore, the concept of cascadability assumes a pivotal role in the context of memory, given that the reciprocal excitation between the Master Laser and the Slave Laser constitutes a fundamental mechanism for implementation.

6.1.1 Cascadability Measurements

To demonstrate the laser model's capability to induce excitation in the subsequent laser, a Master laser was constructed with the capacity to process two inputs. The primary input consisted of the standard pulse utilized throughout the experiment, while the secondary input integrated the feedback signal derived from the Slave laser. To establish a fundamental understanding, temporal traces of both lasers were generated. This approach facilitates a straightforward comparison between the two lasers, offering an "if this, then that" framework without necessitating an exhaustive exploration of the intricate equations governing laser dynamics. The time traces provide a visual representation, allowing for a clear and intuitive assessment of the sequential interactions between the Master and Slave lasers.

In Figure 15, we observe the pivotal role played by the input in influencing the overall cascadability of the system. As demonstrated in the preceding section, the induction of higher peak pulses into the laser results in an increased output peak power. Consequently, introducing a very low-energy signal into the Master laser leads to a diminished peak on the output side, potentially falling below the threshold required to excite the second laser.

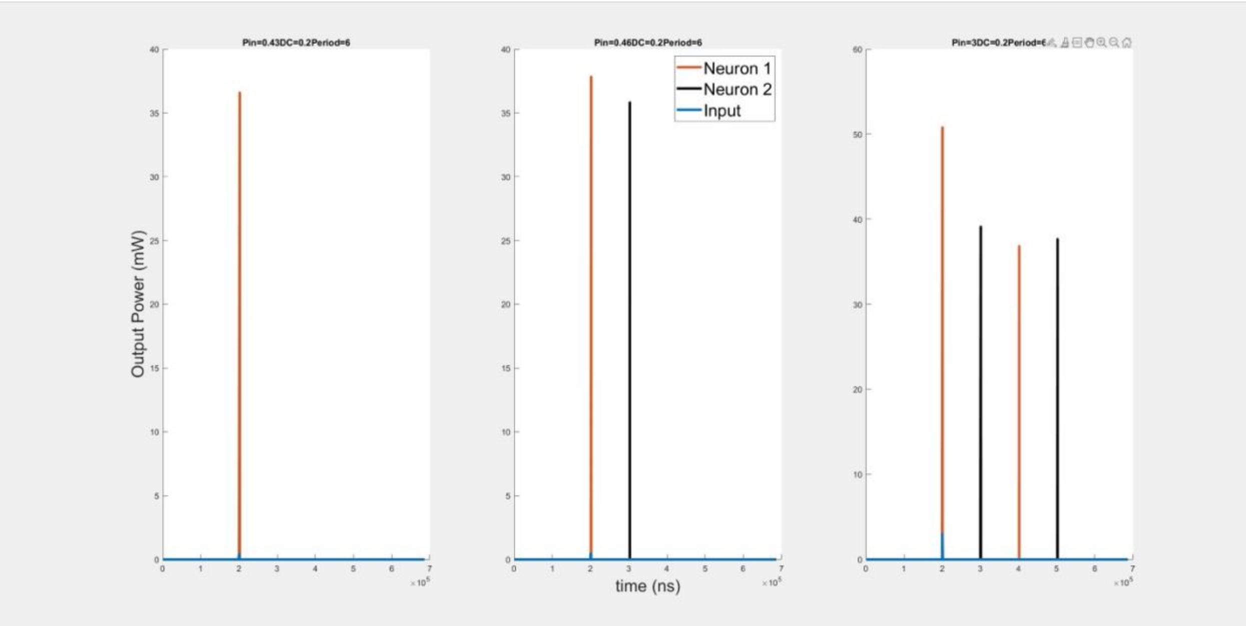

Figure 15: A, B, and C presents three temporal traces of a feedback laser system, where the red lines delineate the temporal evolution of the Master Laser output, and the black lines represent the Slave Laser output. In Panel A, the input pulse marginally reaches the threshold of the Master Laser, proving insufficient to excite the second laser. In Panel B, the input pulse is incrementally heightened, enabling the output pulse to marginally excite the Slave Laser. However, the signal is not sufficiently robust to complete the loop and re-excite the Master Laser. Finally, in Panel C, the input is of sufficient magnitude for the signal to traverse the loop for several cycles.

Nevertheless, as previously observed, the correlation between input peak and output adheres to a logarithmic trend, indicating that beyond a certain point, substantial increases in input peak yield marginal alterations in the output. This poses a inherent challenge in the system, particularly in the context of memory functionality. If the pulse cannot be perpetually regenerated, it does not meet the criterion for being termed memory. Even in cases where temporary preservation of the pulse suffices, the requisite input power is notably high. Implementing such high input power is non-trivial in small-scale hardware configurations and becomes inefficient when considering the scale necessitated for the implementation of millions of neurons to realize a memory system.

An alternative method to augment the energy of the output spike, concurrently offering a solution, involves base current injection. This refers to the current maintaining the laser in the ready-fire state. By elevating the rest state closer to the threshold, even minimal input pulses, previously insufficient to excite the neuron, not only surpass the threshold but also yield a substantially intensified peak. In this configuration of lasers, the strategy entails augmenting the current of the second laser. Consequently, any spike from the master laser, irrespective of its strength, becomes adequate to generate an output in the slave. This ensures a higher peak in the slave laser than the original spike, obviating challenges associated with the re-excitation of the master laser.

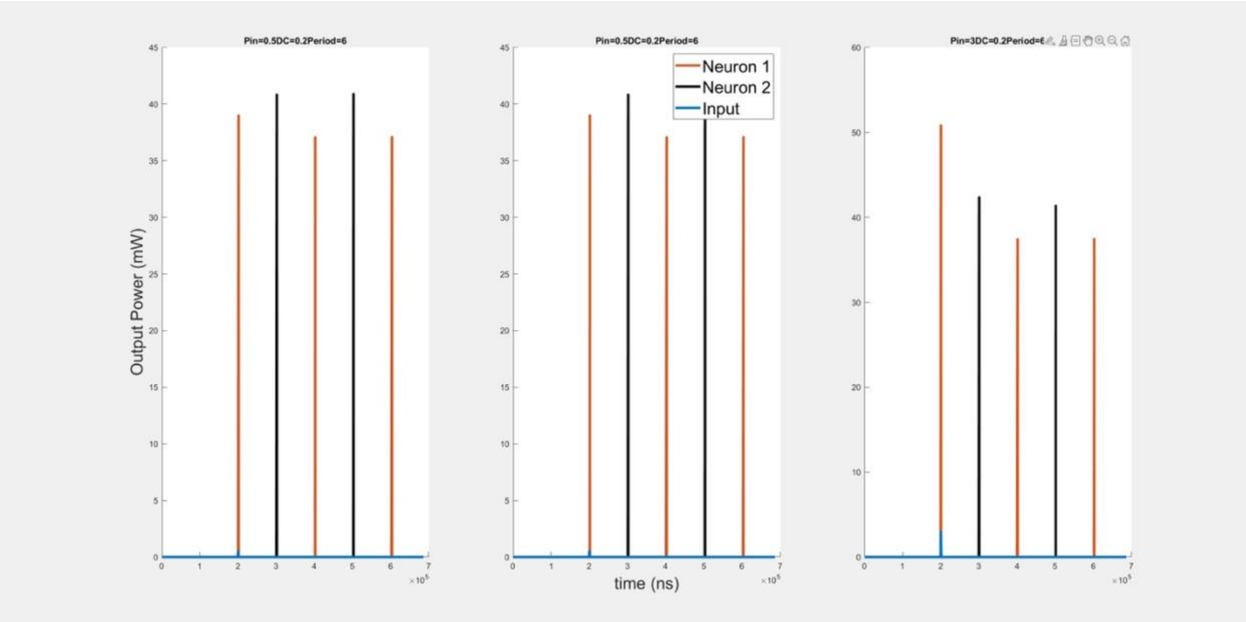

Figure 16: A, B, and C maintain identical configurations to the previous graph, with the sole distinction lying in the I-bias, which is increased by 0.25 mA. This minute increment proves sufficient to transform the system into a viable memory, as the initial spike can now consistently recur at precisely the same intervals of time indefinitely.

6.2 Input Pulse Influence

In the experimental methodology outlined in Chapter 5, the investigation of input pulse dynamics involved a systematic elevation of its peak power alongside the concurrent recording of laser output. Departing from conventional approaches, the focus herein was on the phenomenon of memory, necessitating the comprehensive capture of spikes in their entirety rather than isolated instances. Specifically, attention was directed towards the initial pulse emitted by the master laser in response to the input, the ensuing spike from the slave, and the subsequent occurrence of the second master pulse. This sequencing aimed to elucidate the influence exerted by the slave on the post-cycling spike dynamics.

Subsequent phases of experimentation revealed a notable challenge in attempting to exhaustively measure absorber values. Despite efforts to meticulously gauge each parameter, the task became prohibitively burdensome, yielding marginal insights. Presently, the absorber is configured to a nominal setting of 2 mV; however, it is acknowledged that augmenting absorber levels necessitates heightened power input to sufficiently stimulate neuronal activity, thereby engendering stronger spike manifestations. This amplification in spike strength translates to an augmented energy influx within the system, thereby enhancing the ease with which each laser can trigger the subsequent iteration, thus facilitating enhanced cascadability. In practical applications, the ideal absorber setting should strike a delicate balance, ensuring minimal interference with laser functionality while concurrently minimizing spike peak intensity.

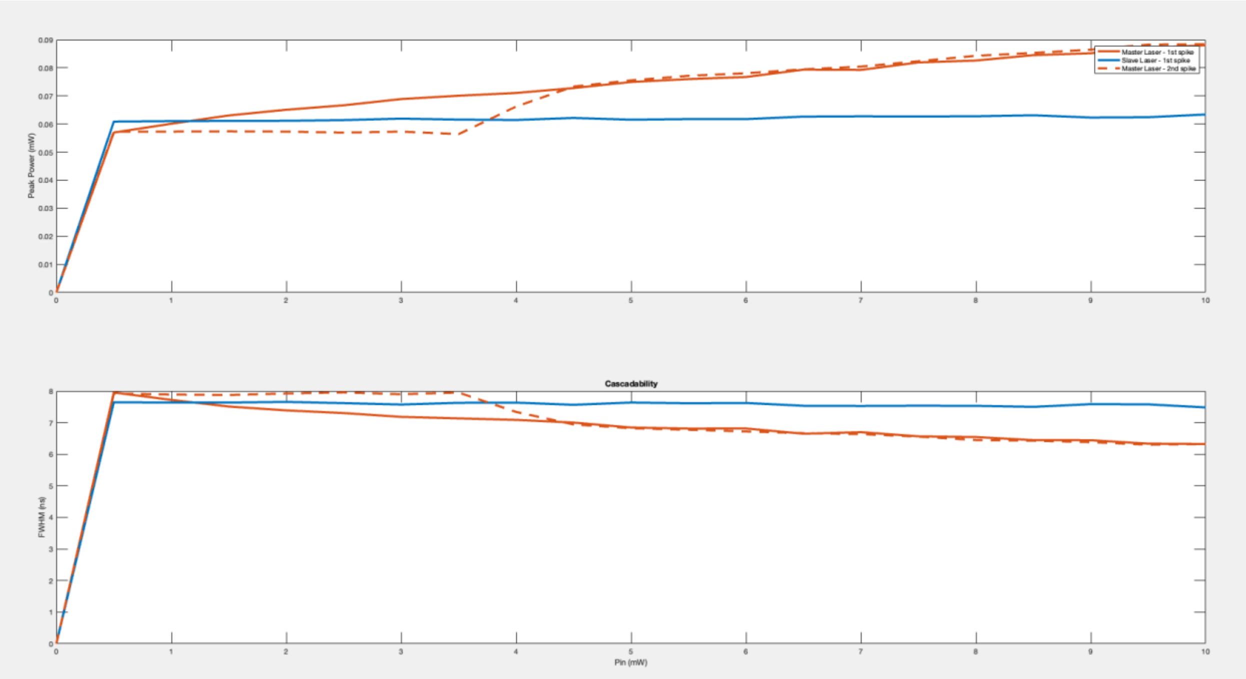

Figure 17: (A) illustrates the relationship between the peak power of the first three spikes and the input power. The red lines represent data from the master laser, while the blue lines depict data from the slave laser. Straight lines denote the first spikes, whereas dotted lines represent the output after the first cycle. (B), the same spikes are depicted, but with a focus on measuring the width of the pulse. The term FWHM (Full-Width-Half-Maximum) is employed as a standard means of quantifying pulse width. FWHM denotes the width of the pulse measured at -3 dB.

As evident from figure 17, the initial spike of the master laser exhibits a gradual increase in tandem with the rise in input power, a trend anticipated based on prior findings outlined in the preceding chapter. However, notably, the second pulse maintains a consistent power level throughout the duration of measurement. This phenomenon arises due to the non-linear scaling of the output spike with respect to the input, but it increases with a slower rate of change. Given that this output serves as the input for the second laser, minor fluctuations of this nature are unlikely to yield discernible discrepancies. Furthermore, in accordance with the first law of physics, which stipulates the conservation of energy, it follows that the peak power of any spike inversely correlates with the width of the pulse. Consequently, the overall energy remains conserved despite variations in individual spike characteristics.

Following this line of reasoning, it would be anticipated that the second spike of the master laser remains consistent, given that the slave laser's output maintains a steady peak power, which serves as input to the master. However, it is crucial to consider the underlying dynamics of the system. The red lines, representing the overall population of the laser at any given time, reflect a complex interplay of factors. For the population to revert to its relaxed state, a certain duration of time is requisite.

In the context where the two lasers are in close proximity and accounting for the velocity of light propagation, it becomes evident that the slave's spike reaches the master before the total population has had adequate time to return to its relaxed state. Consequently, there exists a finite period wherein the population within the master laser cavity remains in a non-relaxed state. Notably, the magnitude of this effect is contingent upon the peak power; higher peaks entail a slower reset process.

Observations from figure 17 corroborate this phenomenon, particularly evident around the 4 mW mark, where an increase in the second spike of the master laser is discernible. This augmentation is attributable to the combination of input from the slave laser and the residual population existing within the master laser cavity prior to completing the reset period.

6.3 Multiplse Spikes

In neurotrophic computing, spike encoding stands as a fundamental aspect of information processing. Inspired by the operation of biological neural networks, wherein information is conveyed through the generation of action potentials or "spikes," neurotrophic computing endeavors to emulate this mechanism for efficient computation. Spike encoding enables the representation and transmission of information in the form of discrete, precisely timed pulses. Through sophisticated encoding schemes[12], such as *rate-based or temporal coding*, neural networks can efficiently encode and process complex information.

The exploration in the preceding chapter naturally prompted a pertinent query: what ensues when the input comprises not a solitary pulse, but rather a train of pulses? This query stems from the recognition that efficient information transmission between neurons necessitates more than a single pulse per clock cycle. Encoding mechanisms play a pivotal role in facilitating communication within systems. By maximizing the injection of pulses within each clock period, the potential for information transmission is exponentially increased.

To obtain meaningful data, it became imperative to enhance the spatial separation between the two lasers. This adjustment served the purpose of elongating the delay required for a pulse to traverse from one laser to another and mitigating the risk of injecting spikes while the preceding one was still in the process of resetting. The experimental protocol entailed measurements conducted for both two consecutive input pulses and three, thereby affording a comprehensive examination of the system's response dynamics under multiple inputs.

6.3.1 Two Spikes

For precise measurement of results, we adopted a methodological approach centered on utilizing the middle spikes as a reference for peak power. This decision was motivated by insights gleaned from figure 18, which revealed instances where both spikes persisted for a couple of cycles. However, the crux lay in consistently measuring the same spikes across multiple cycles, thereby serving as a reliable indicator of successful memory retention.

By anchoring our analysis to the middle spikes, we aimed to mitigate potential variability arising from transient fluctuations or irregularities in spike persistence. This approach ensured consistency and comparability in our measurements, thereby facilitating a more robust evaluation of memory performance within the system.

The graph suggests that, under the specified conditions, the memory function operates effectively, preserving both spikes indefinitely at a certain input power (Pin) level. The precise Pin value may vary due to fluctuations in input pulse characteristics. However, the crucial insight lies in comprehending the underlying mechanisms driving this phenomenon. Consequently, engineering a solution that provides the system with more flexibility becomes imperative. This entails devising strategies to enhance the system's adaptability, thereby affording it greater latitude in accommodating variations in input parameters.

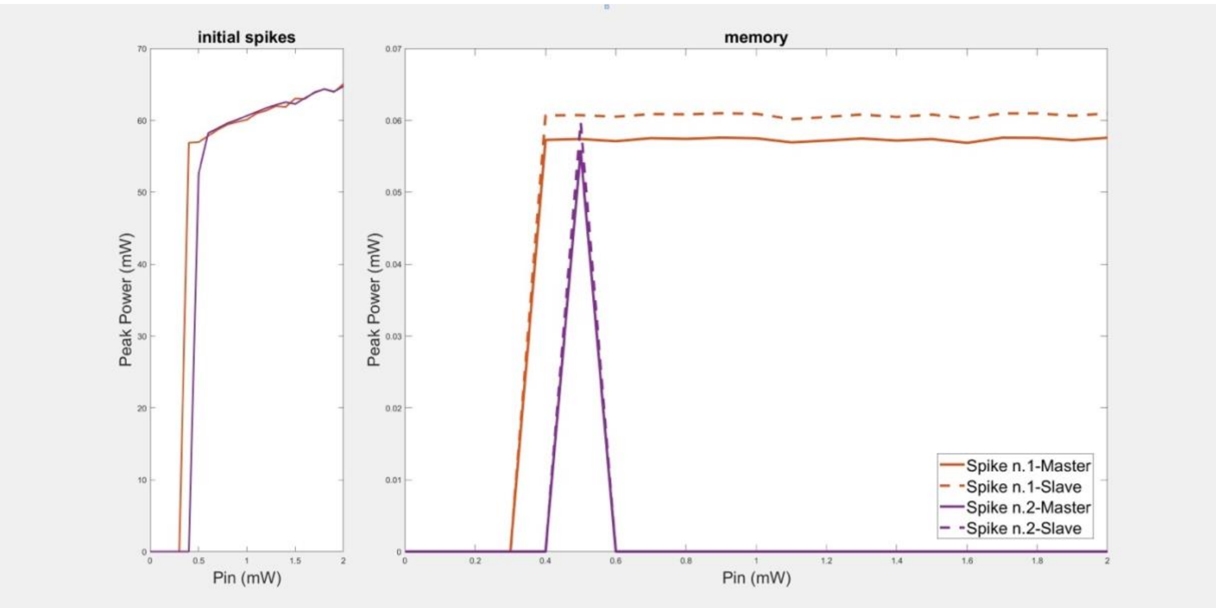

Figure 18: Panel (A) illustrates the peak power of the two initial spikes, represented by the red and purple lines. Panel (B) depicts the spikes occurring within the memory system, with solid lines denoting the master laser and dotted lines representing the slave laser. The graph highlights that the second spike (purple) can only be preserved within the memory under highly specific conditions. This observation serves as a precursor to the subsequent demonstration provided in Graph 10.2, where the requisite values for successful preservation of the second spike are elucidated.

A recurring observation throughout the measurements conducted thus far suggests that elevating the input power correlates with an increase in pulse peak power, consequently prolonging the timing due to the laser's reset mechanism. Figure 12 exemplifies how stronger pulses, in terms of their peak power, correspond to extended refractory periods. This interplay between input power and refractory period implies that manipulating the input effectively influences the laser's refractory period.

In the context of memory, as depicted in Figure 19b, the proximity of pulses is such that while they do not significantly disrupt the initial spikes of the Master's laser, the second pulse gradually diminishes after the first iteration. This phenomenon is contrasted with the observations from Figure 19c, where the input pulse's low magnitude fails to induce a notable increase in the laser's refractory period. Consequently, both spikes are sustained until the conclusion of the simulated time period. These findings underscore the intricate relationship between input power, refractory period dynamics, and the sustainability of spike reproduction within the memory framework.

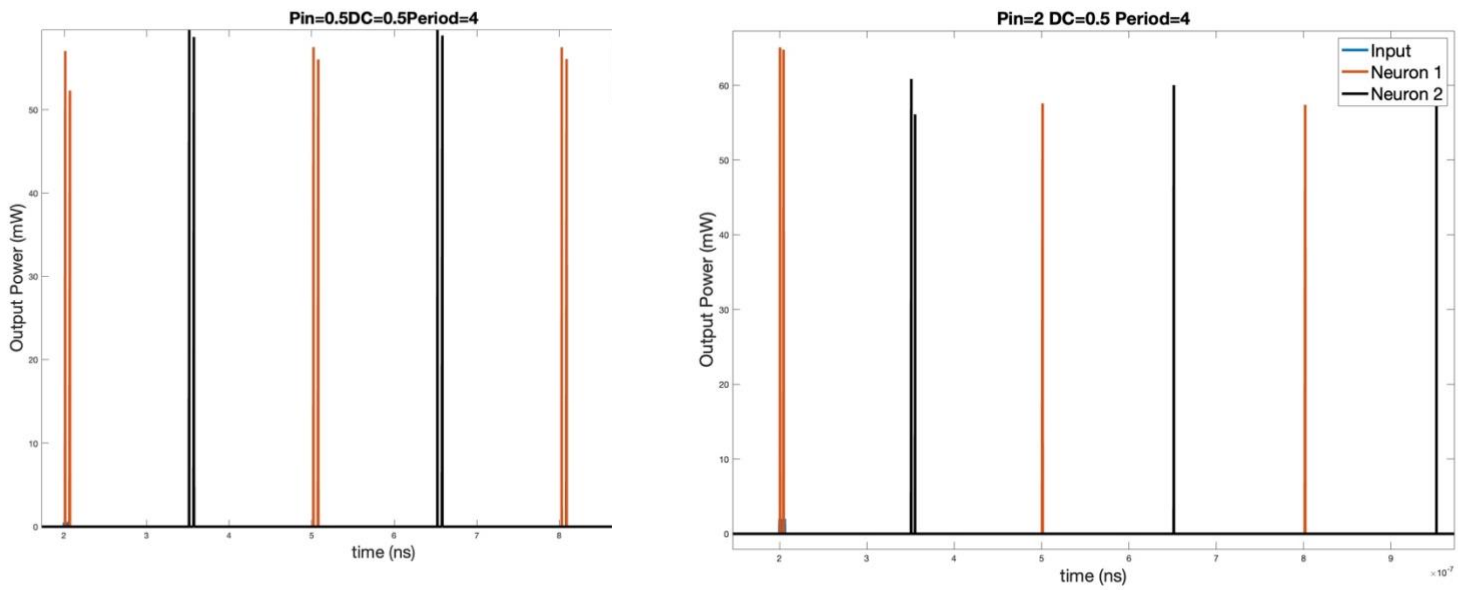

Figure 19:Panels (A) and (B) present time traces of the two lasers. The titles of the graphs describe the specific characteristics of the input pulses. As anticipated from the findings of Graph 10.1, when the input power (PIN) is set at 0.5 MW, the spike can reoccur in the memory for an extended period. However, for any other value, such as 2 MW, as illustrated, the memory fails to reproduce both spikes after a cycle.

6.3.2 Three Spikes

Now that a baseline behavior has been established regarding the response to two pulses, a third pulse was introduced to ascertain if any discernible differences would emerge. However, as observed in Figure 20, the system's behavior remains consistent. The initial spikes exhibit a high probability of reproduction, while the third spike may be susceptible to loss over time, particularly when the input peak exceeds a certain threshold. An noteworthy observation is that the data suggests the power conducive to memory operation is not fixed but rather a range. Nevertheless, this revelation alone does not provide a definitive solution to the underlying mechanism, as the range remains relatively narrow and subject to alteration with the addition of more pulses. Further investigation is warranted to elucidate the intricacies of the system's response to varying input parameters.

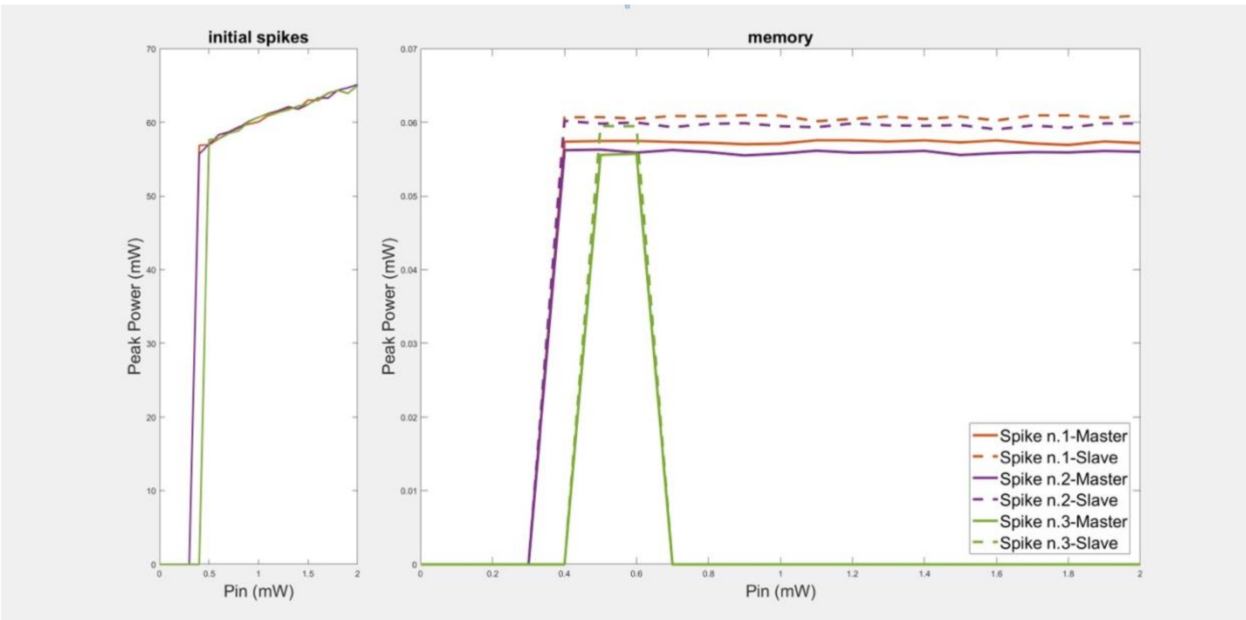

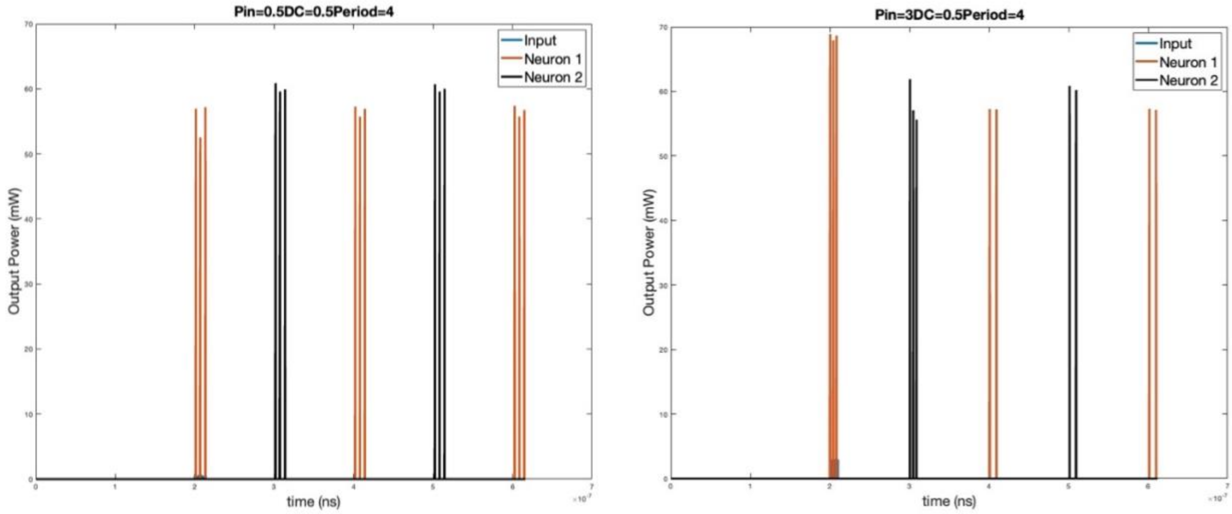

Figure 20: **exhibits identical results to those of Graph 10, following the same methodology with the only distinction being a slight increase in the accepted range of input power (PIN).**

An intriguing observation stemming from the analysis of Graphs 17 and 18 is the disparate outcomes regarding the amplification or destruction of subsequent pulses. While in the former case, the second pulse was capable of amplifying the spike utilizing residual energy from the preceding pulse if it occurred during the reset phase, in the latter case, consecutive pulses not only failed to amplify but also led to the destruction of subsequent ones. Although not explicitly anticipated in the experimental design, this phenomenon finds explanation in Chapter 5, where it is states *"revisiting Figure 2, we observe that the refractory period occurs only when the membrane potential— or in our case, the population— dips below the* *relaxation state. When the input power maintains a constant value, the laser seldom dips below the resting state threshold, enabling it to spike more rapidly."*

Figure 17 illustrates how an input characterized by minimal delay (close to 0 ps) approximates a continuous input, while even a slight delay may precipitate entry into the refractory period, during which the population remains significantly below the relaxed state. This observation highlights the insufficiency of the same input to excite the laser when occurring within the refractory period.

6.3.3 Solution

In order to furnish compelling evidence regarding the influence of pulse separation distance, two additional graphs were generated. These graphs were meticulously crafted to maintain identical configurations of the laser system while systematically altering the Pulse Period (Inter-Spike Interval, ISI) and the Duty Cycle (DC) to precise values.

Isi = 8ps & dc = 0.25 => Dealy = 8ps – 8*0.25ps = 6ps

These adjustments were instrumental in scrutinizing the impact of varying pulse separation distances on the system's response dynamics. By holding all other parameters constant and selectively manipulating the ISI and DC, the experimental setup afforded a controlled environment conducive to isolating the effects of pulse spacing. The resulting data provided invaluable insights into the relationship between pulse separation distance and the system's performance metrics, thereby bolstering our understanding of the underlying mechanisms governing pulse propagation and interaction within the laser system.

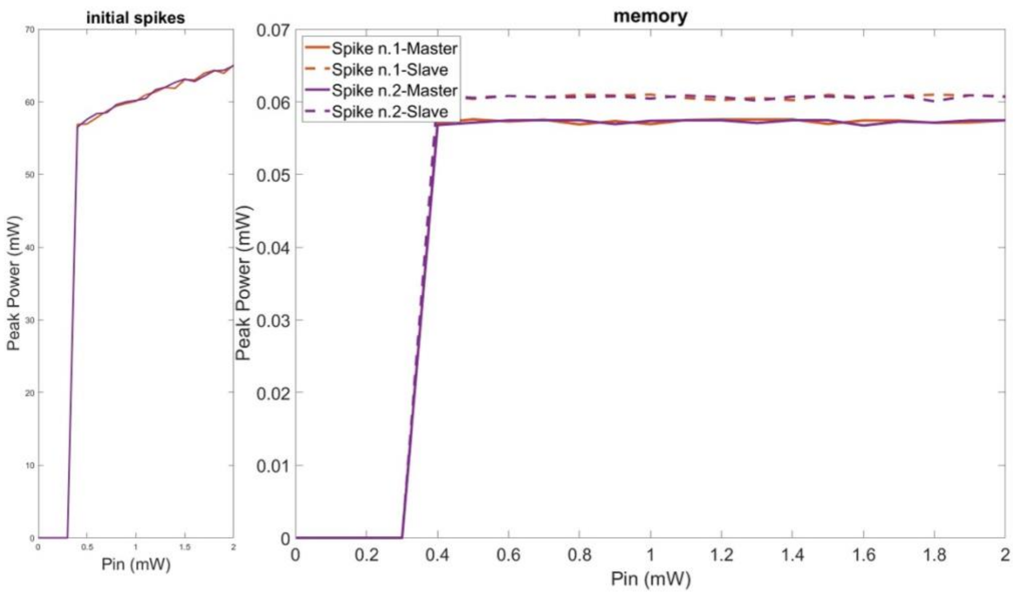

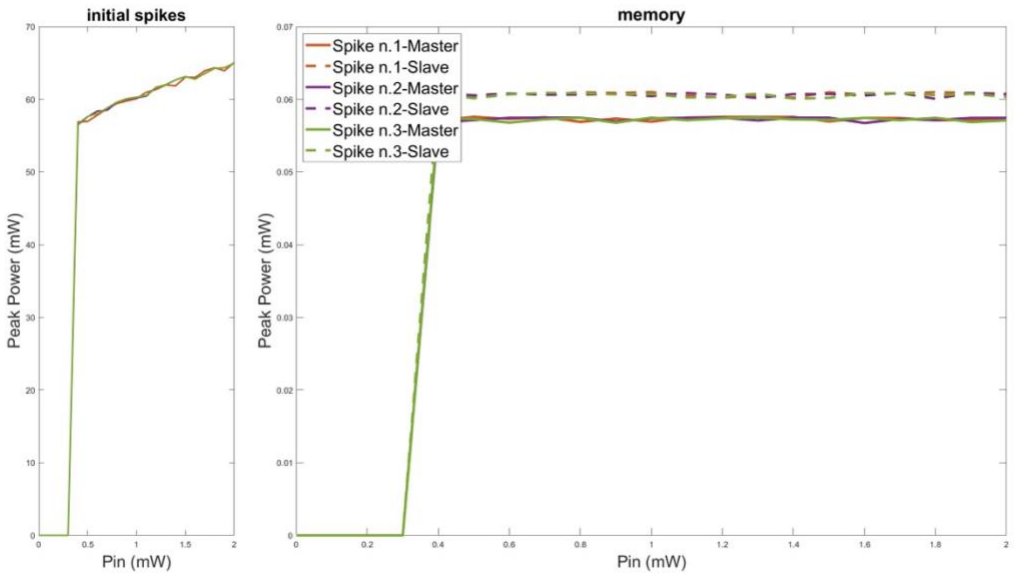

Figure 21 A and B proving how the slight Delay increase can provide a solution for the memory

6.4 Pulse Distance

The preceding chapter's findings underscored the detrimental effects of injecting pulses too closely together in terms of their timing, which posed challenges for pulse regeneration. However, it was observed that the initial pulses emitted by the master laser exhibited normal firing behavior. Consequently, solely measuring these initial pulses could yield misleading data regarding memory functionality. To address this issue, the focus of this chapter was directed towards determining the optimal spacing between pulses to circumvent the refractory period.

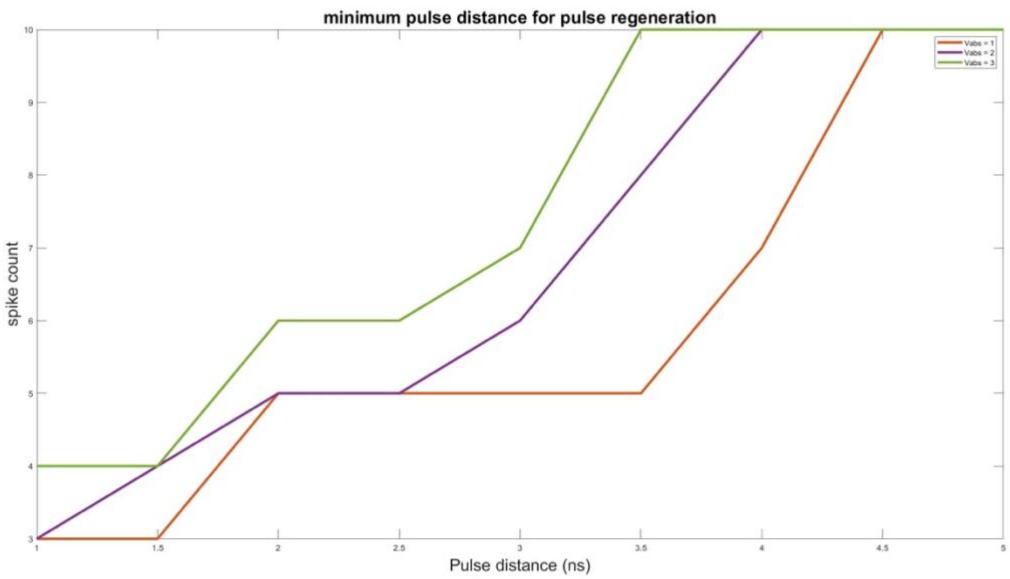

Figure 22 Minimun distance between pulses relative to the desired number of spikes

The measurements were conducted by utilizing a new variable in the Matlab simulation, namely the pulse distance while setting period and duty cycle equal to 1. This variable was systematically increased while simultaneously graphing the spike count in each scenario. This approach allowed for the determination of the minimum distance required for the memory to regenerate a specific quantity of spikes. Through this iterative process, the critical threshold at which pulse spacing becomes sufficient for reliable spike regeneration within the memory system was identified. The resultant data provided valuable insights into the intricate relationship between pulse separation distance and memory performance, thereby advancing understanding of the underlying mechanisms governing memory functionality within the laser system.

In real-life systems, the generation of such precise pulses may pose a considerable challenge. However, modern devices afford users the capability to manipulate the period of the pulse and the duty cycle. By adjusting these two parameters, it becomes feasible to generate pulses with varying distances between them. This can be achieved through the following method:

From the previous simulation with the pulse distance:

$$Isi = 1ps\ and\ DC = 1$$

Thus by adding the old period and the delay we get the new period

$$ISI' = pulse\ delay + ISI = pulse\ delay + 1$$

Since the previous period (which was set to 1) is the current active cycle we can write

$$ISI' * DC' = Isi \rightarrow DC' = \frac{1}{pulse\ delay + 1},$$

6.5 Lasers Capacity

The system's capacity denotes the quantity of consecutive spikes the memory can retain without experiencing any losses. As previously alluded to, when the lasers are in close proximity, signal propagation between the master and slave lasers occurs almost instantaneously. Consequently, in scenarios involving multiple spikes, there exists the potential for the first spike emitted by the master laser to return before the completion of the initial train of inputs.

The subsequent figure illustrates the anticipated output of the memory system. Notably, it is readily discernible that the initial spikes of both the master and slave lasers are distinguishable. This observation underscores the adequacy of the delay between pulses to accommodate the spiking of all pulses and facilitate their transmission to the slave laser and subsequent return. It is noteworthy that in this particular configuration, the delay was deliberately exaggerated to emphasize its significance. However, this approach results in a significant amount of idle time during which the master laser remains inactive. Given the scale of practical neural networks, such a delay could compound into a considerable period, potentially impeding overall system efficiency.

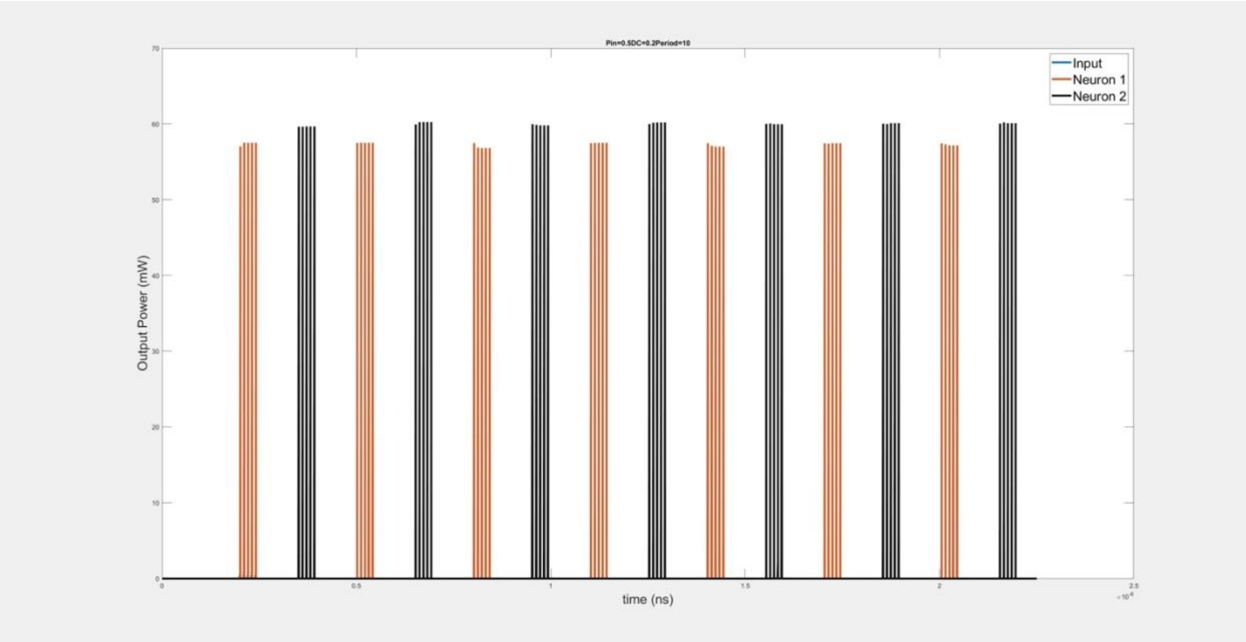

Figure 23: depicts a time capture of the memory system with a significant delay between the lasers. Although the spikes are distinctly separated, the duration of the delay between them exceeds that of the spike train itself. This implies that there is ample space between consecutive spike trains, such that another spike train could easily fit in between them.

A more efficient way to use this delay is to make the slave laser spike while the master is still processing the input pulses, but not fast enough so that the master receives the signal back before it finishes. Figure 24 shows this delay could be used to secure maximum efficiency while still having functional memory. The spikes look very interplexed, however by just focusing on one of the lasers, can be clear that the memory still functions perfectly.

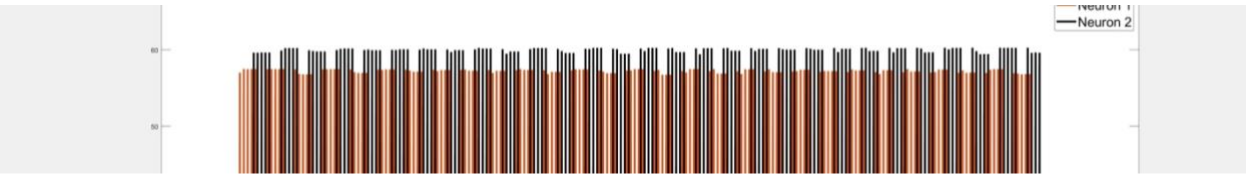

Figure 24: illustrates the functionality of the memory system, even in scenarios where the slave laser emits spikes before the master laser completes processing the input. By separately counting the spikes of the master laser (represented by red lines), it is evident that all five spikes are successfully saved in the memory. This observation underscores the robustness and reliability of the memory system in capturing and retaining spike data, irrespective of the timing discrepancies between the master and slave lasers.

It is imperative to prevent the occurrence of the slave laser's output reaching the master laser before the input spike train is complete. Such a scenario introduces unwanted spikes into the spike train, thereby exacerbating the problem. This effect becomes even more pronounced when considering multiple cycles, as each unwanted spike in the master laser triggers a corresponding spike in the slave laser. Consequently, in subsequent cycles, additional unwanted spikes will occur, leading to the gradual accumulation of random spikes in the memory. This phenomenon renders the memory system increasingly opaque and ultimately compromises its decoding capabilities.

To underscore the significance of this concept, the ensuing figure employs an exaggerated portrayal of minimal travel delay. This depiction serves to vividly illustrate the profound impact of delay on the memory's capacity, emphasizing its pivotal role in shaping the system's performance and reliability.

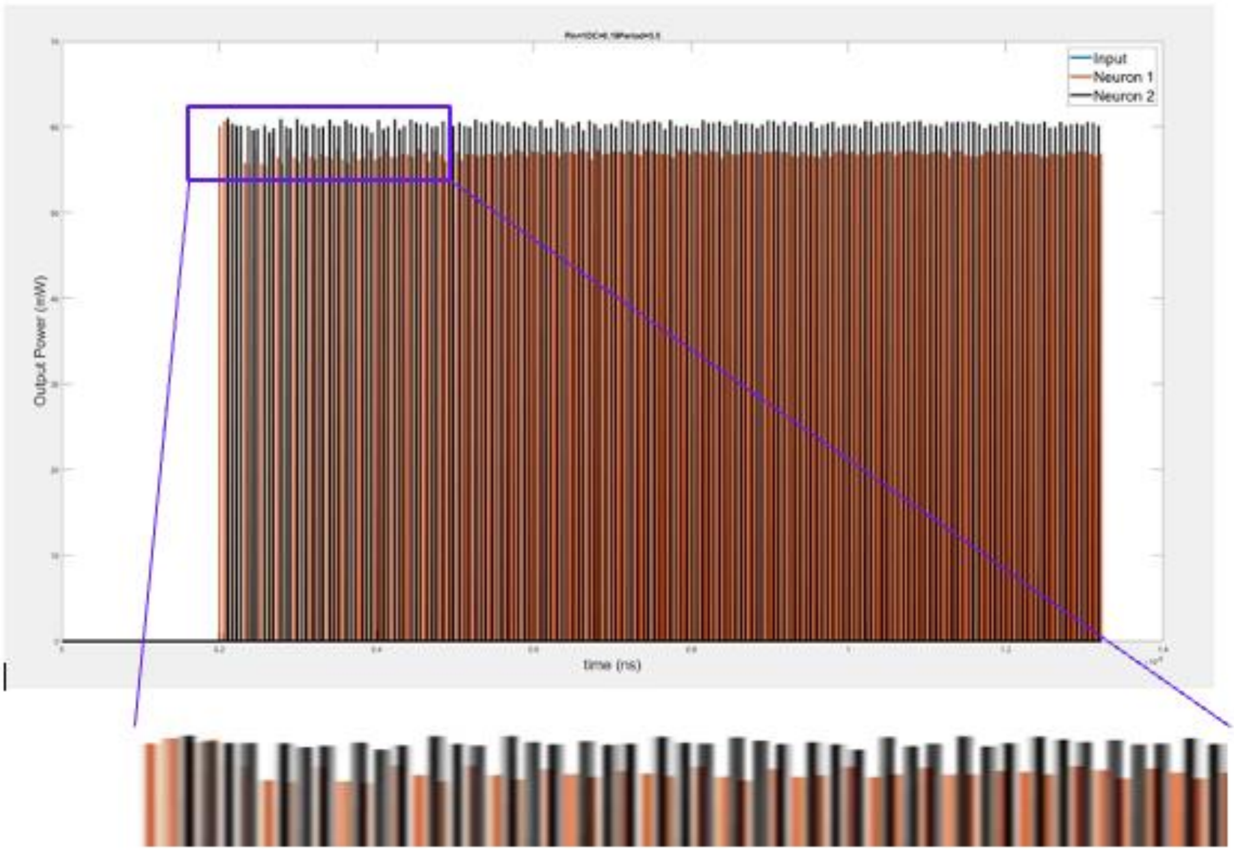

Figure 25: shows how the delay can cause the memory to behave randomly and the snowball effect that one uwanted spike can have in the overall functionality

To precisely determine the optimal delay required for maximal efficiency and reliability, taking into account the memory's capacity, measurements were conducted on the master laser. This involved systematically decreasing the delay and plotting the last saved value at which the system's spike count remained consistent across multiple iterations. Figure 26 illustrates a linear relationship between the delay and the memory's capacity, indicating that increasing the delay enables more spikes to be stored in the memory. Mathematically, this can be substantiated by the condition that a functional memory necessitates the master laser to not receive a spike while processing the input train.

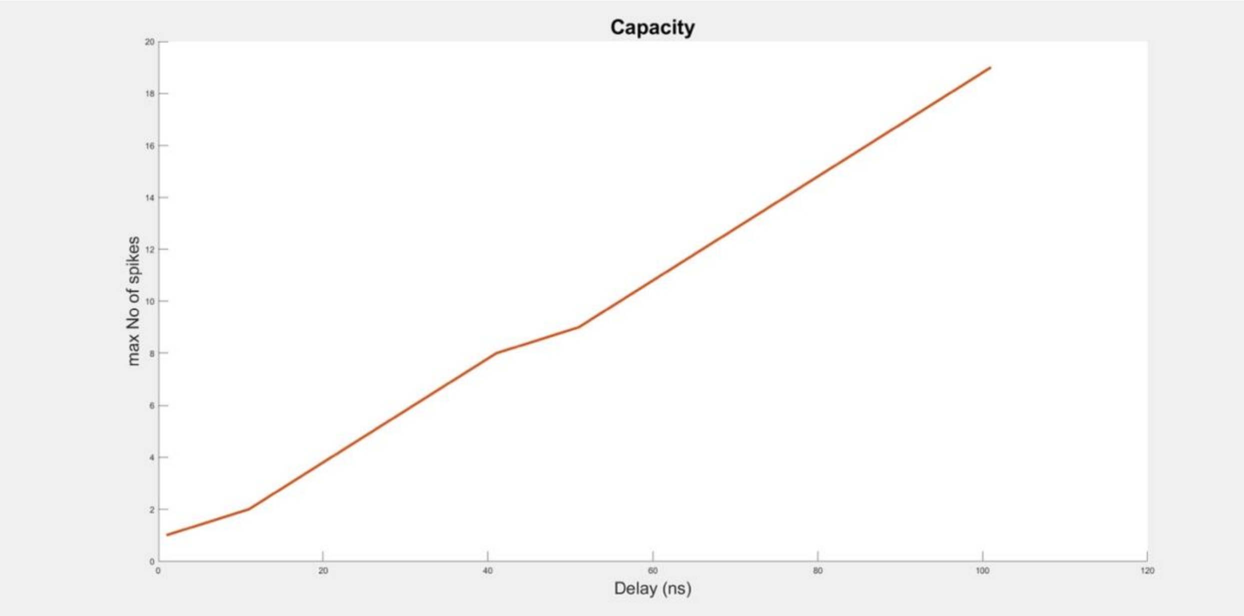

Figure 26: The capacity of the memory to save consecutive spikes, showing a linear relationship with the delay between the two lasers. As the delay increases, there is a proportional increase in the memory's spike storage capacity. This linear trend highlights the direct influence of delay on spike retention within the memory system.

The time for the spike train can be described by the following equation.

$$\Delta p = ISI * N$$

Where Δp describes the total time it takes for the input to be processed, ISI is the period of one input, which also includes the negative period, and N the total amount of spikes.

That means, the total cycle delay:

$$delay_{totatl} = delay_{travel} * 2$$

should surpass the total time:

$$ISI * N = delay_{travel} * 2 \rightarrow \frac{ISI * N}{2} = delay\_travel$$

7

Conclusion

In this thesis, the primary objective was to demonstrate the potential of utilizing lasers for the implementation of Neuromorphic Hardware, drawing parallels between their inherent characteristics and those of biological neurons, while exploring the feasibility of memory implementation. Through rigorous investigation, it has been revealed that Semiconductor Optical Amplifiers (SOAs) exhibit behaviors akin to the Leaky Integrate-and-Fire (LIF) model, offering a compelling approximation of biological neuron functionality. However, it is imperative to acknowledge current limitations, particularly concerning the challenges associated with cost and temperature management, which have been overlooked in this study. Addressing these limitations holds the key to realizing the full potential of neural network hardware based on laser technology. Moreover, as demands for efficient and scalable computing solutions continue to escalate, it becomes increasingly imperative to direct further research towards the development of laser-based Neuromorphic Hardware. By overcoming existing barriers and refining laser-based neural network architectures, we can pave the way for innovative solutions capable of meeting the evolving demands of contemporary computing paradigms, thus ushering in a new era of computational efficiency and versatility.

References

1. H. Amin and R. Fujii, "Spike train decoding scheme for a spiking neural network," 2004 IEEE International Joint Conference on Neural Networks (IEEE Cat. No.04CH37541), Budapest, Hungary, 2004, pp. 477-482, doi: 10.1109/IJCNN.2004.1379956.
2. von Neumann, J. (1982). First Draft of a Report on the EDVAC. In: Randell, B. (eds) The Origins of Digital Computers. Texts and Monographs in Computer Science. Springer, Berlin, Heidelberg
3. Heemskerk, Jan NH. "Overview of neural hardware." Neurocomputers for brain-style processing. Design, implementation and application (1995).
4. R.C. Merkle, "Energy limits to the computational power of the human brain" Foresight Update No. 6 August 1989
5. Herculano-Houzel S. The human brain in numbers: a linearly scaled-up primate brain. Front Hum Neurosci. 2009 Nov
6. J.B Furness Types of neurons in the enteric nervous system Journal of the Autonomic Nervous System Volume 81, Issues 1–3 2000 Pages 87-96 ISSN 0165-1838
7. Rodolfo R. Llinás, "I of the Vortex: From Neurons to Self", The MIT Press ISBN electronic: 9780262278454
8. HODGKIN AL, HUXLEY AF, KATZ B. Measurement of current-voltage relations in the membrane of the giant axon of Loligo. J Physiol. 1952 Apr;116(4):424-48. doi: 10.1113/jphysiol.1952.sp004716. PMID: 14946712; PMCID: PMC1392219.
9. Hodgson, Norman, and Horst Weber. Optical resonators: fundamentals, advanced concepts and applications. Springer Science & Business Media, 2013.
10. Prucnal, P.R., & Shastri, B.J. (Eds.). (2017). Neuromorphic Photonics (1st ed.). CRC Press. https://doi.org/10.1201/9781315370590
11. Dubbeldam, J. L. A., & Krauskopf, B. (1999). Self-pulsations of lasers with saturable absorber: dynamics and bifurcations. Optics Communications, 159, 325-338, https://doi.org/10.1016/S0030-4018(98)00568-9
12. Simon Thorpe, Arnaud Delorme, Rufin Van Rullen,Spike-based strategies for rapid processing,Neural Networks,Volume 14, Issues 6–7,2001,Pages 715-725,ISSN 0893-6080, https://doi.org/10.1016/S0893-6080(01)00083-1
13. Yamada, M. and Hiratsuka, A. (1993) A Study of the Concept of Environment—In View of "IN-DER-WELT-SEIN" by M. Heidegger. Journal of Environmental Systems Research, 21, 110-113.
14. N. S. Kim *et al*., "Leakage current: Moore's law meets static power," in *Computer*, vol. 36, no. 12, pp. 68-75, Dec. 2003, doi: 10.1109/MC.2003.1250885. keywords: {Leakage current;Moore's Law;Energy consumption;Frequency;Equations;Microprocessors;Threshold voltage;CMOS logic circuits;Power dissipation;CMOS technology},

[i] Synapses: the connections between neurons. The point where the dendrites meet the axon terminals.

[ii] Membrane potential: refers to the difference in electrical charge that exists across the cell membrane of a neuron.

[iii] Second-order DE: an equation that involves the second derivative of a dependent variable

[iv] In the context of dynamical systems and differential equations, the dot notation on top of variables indicates the derivative of the variable with respect to time.